Integrated Ocean Drilling Program
Expedition 345 Scientific Prospectus

Hess Deep Plutonic Crust

Exploring the plutonic crust at a fast-spreading ridge: new drilling at Hess Deep

Kathryn Gillis
Co-Chief Scientist
School of Earth and Ocean Sciences
University of Victoria
Victoria, Canada

Jonathan E. Snow
Co-Chief Scientist
Department of Earth and Atmospheric Sciences
University of Houston
Houston, Texas
USA

Adam Klaus
Expedition Project Manager/Staff Scientist
Integrated Ocean Drilling Program
Texas A&M University
College Station, Texas
USA

Published by
Integrated Ocean Drilling Program Management International, Inc.,
for the Integrated Ocean Drilling Program

Publisher's notes

Citation:
Gillis, K., Snow, J.E., and Klaus, A., 2012. Hess Deep plutonic crust: exploring the plutonic crust at a fast-spreading ridge: new drilling at Hess Deep. *IODP Sci. Prosp.,* 345. doi:10.2204/iodp.sp.345.2012

Distribution:
Electronic copies of this series may be obtained from the Integrated Ocean Drilling Program (IODP) Scientific Publications homepage on the World Wide Web at **www.iodp.org/scientific-publications/.**

This publication was prepared by the Integrated Ocean Drilling Program U.S. Implementing Organization (IODP-USIO): Consortium for Ocean Leadership, Lamont-Doherty Earth Observatory of Columbia University, and Texas A&M University, as an account of work performed under the international Integrated Ocean Drilling Program, which is managed by IODP Management International (IODP-MI), Inc. Funding for the program is provided by the following agencies:

National Science Foundation (NSF), United States

Ministry of Education, Culture, Sports, Science and Technology (MEXT), Japan

European Consortium for Ocean Research Drilling (ECORD)

Ministry of Science and Technology (MOST), People's Republic of China

Korea Institute of Geoscience and Mineral Resources (KIGAM)

Australian Research Council (ARC) and GNS Science (New Zealand), Australian/New Zealand Consortium

Ministry of Earth Sciences (MoES), India

Disclaimer

This IODP *Scientific Prospectus* is based on precruise Science Advisory Structure panel discussions and scientific input from the designated Co-Chief Scientists on behalf of the drilling proponents. During the course of the cruise, actual site operations may indicate to the Co-Chief Scientists, the Staff Scientist/Expedition Project Manager, and the Operations Superintendent that it would be scientifically or operationally advantageous to amend the plan detailed in this prospectus. It should be understood that any proposed changes to the science deliverables outlined in the plan presented here are contingent upon the approval of the IODP-USIO Science Services, TAMU, Director in consultation with IODP-MI.

March 2012

Abstract

Integrated Ocean Drilling Program Expedition 345 (11 December 2012 to 10 February 2013) will be the second offset drilling program at the Hess Deep Rift to study crustal accretion processes at the fast-spreading East Pacific Rise (EPR). The expedition will take advantage of well-surveyed crustal exposures to recover the first cores of young, primitive plutonic rocks that comprise the lowermost ocean crust. The principal objective for drilling at Hess Deep is to test competing hypotheses of magmatic accretion and hydrothermal processes at fast-spreading mid-ocean ridges. These hypotheses make predictions that can only be tested with drill core, including the presence or absence of modally layered gabbro, the presence or absence of systematic variations in mineral and bulk rock compositions, and the extent and nature of hydrothermal alteration and deformation. With detailed petrological, chemical, and structural data for cores of deep, primitive gabbros, we will be able to address fundamental questions, such as, What proportion of the plutonic lower crust is constructed through crystal subsidence, and what proportion is constructed through in situ crystallization? How is melt transported from the mantle through the crust? What is the origin and significance of layering? How, and how fast, is heat extracted from the lower plutonic crust? What are the fluid and geochemical fluxes in the EPR lower plutonic crust?

The highest priority for drilling at the Hess Deep Rift will be to sample one or more 100 to ≥250 m long sections of primitive gabbroic rocks. Three primary drill sites have been identified; however, if coring is proceeding well in the first or second of these sites, it will be continued as long as possible in order to obtain the longest possible continuous sample. The alternate site is located near Ocean Drilling Program Site 894, where shallow-level gabbros are exposed. This plan differs slightly from Proposal 551, as there is no alternate site in upper mantle peridotite. Drilling and coring operations are anticipated to be challenging during the Hess Deep expedition because of water depths >4800 m, a thin sediment cover, and, potentially, unstable basement formations.

Schedule for Expedition 345

Integrated Ocean Drilling Program (IODP) Expedition 345 is based on IODP drilling Proposals 551 and 551-Add (available at **iodp.tamu.edu/scienceops/expeditions/hess_deep.html**). Following ranking by the IODP Science Advisory Structure, the ex-

pedition was scheduled for the R/V *JOIDES Resolution,* operating under contract with the U.S. Implementing Organization (USIO). At the time of publication of this *Scientific Prospectus,* the expedition is scheduled to start in Puntarenas, Costa Rica, 11 December 2012, and end in Balboa, Panama, 10 February 2013. A total of 46 days will be available for the drilling, coring, and downhole measurements described in this report (for the current detailed schedule, see **iodp.tamu.edu/scienceops/**). The supporting site survey data for Expedition 345 are archived in the **IODP Site Survey Data Bank.** Further details about the facilities aboard the *JOIDES Resolution* and the USIO can be found at **www.iodp-usio.org/.**

Introduction

The accretion of new ocean crust at mid-ocean-ridge spreading centers is one of the fundamental processes of Earth evolution. Understanding the nature of the crust and mantle and the underlying geologic processes that form them is an ongoing fundamental justification for drilling in the ocean basins (Hess, 1960; Ocean Drilling Program [ODP] science plan [**www.odplegacy.org/program_admin/long_range.html**]; IODP Initial Science Plan [**www.iodp.org/isp/**]). The ocean crust forms by solidification of basaltic melts produced by decompression melting in the mantle and subsequent modification during delivery to the lithosphere (see review by Klein, 2007). These basaltic melts evolve through complex processes of crystallization and mechanical deformation, most of which take place within the first million years or so of lithospheric evolution (see Coogan, in press, for a broad overview)

Studies of ophiolites (Anonymous, 1972; Nicolas, 1989) provide a framework for understanding the accretion and evolution of ocean crust and, as in the case of this expedition, provide nearly all of the extant observations of the type of crust under study. Ophiolite studies, however, suffer from a lack or uncertainty of geologic context, including such fundamental parameters as spreading rate, orientation of structures with respect to the ridge and stratigraphic level, and tectonic setting. Ophiolite studies provide a useful overall framework for understanding the genesis and architecture of the ocean crust, but only direct observation of modern ocean crust can inform a definitive understanding.

The state of ocean drilling into the igneous basement is summarized in Figure **F1,** where sites are organized by crustal depth and spreading rate. Two sites in particular, Sites 504 and 1256, have achieved significant penetration, generating a wealth of in-

formation regarding the igneous, thermal, and hydrologic state of the upper ocean crust, formed intermediate and fast spreading rates, respectively. Although the transition into the upper plutonic crust was drilled at Site 1256, the lower plutonic crust has not yet been sampled in an intact hole.

A complementary approach to sample the lower crust is to take advantage of "tectonic windows," where lower crust and upper mantle exposures are unroofed by tectonic processes (Offset Drilling Working Group, 1994), thus bypassing the upper crust entirely. The offset drilling approach has had varying success in terms of hole penetration (Fig. **F1**) but has yielded significant scientific return at Hess Deep (Gillis, Mével, Allan, et al., 1993), the Southwest Indian Ridge (Robinson, Von Herzen, et al., 1989; Dick, Natland, Miller, et al., 1999), and the Mid-Atlantic Ridge (Cannat, Karson, Miller, et al., 1995; Kelemen, Kikawa, Miller, et al., 2004; Blackman, Ildefonse, John, Ohara, Miller, MacLeod, and the Expedition 305/306 Scientists, 2006).

The principal objective of Expedition 345 is to sample the lower levels of young plutonic crust that formed at the fast-spreading East Pacific Rise (EPR), filling in a major lithologic gap (dotted oval in Fig. **F1**). The expedition will take advantage of the offset drilling approach by initiating holes directly into exposures of relatively deep lower crustal rocks at the Hess Deep Rift. Expedition 345 will build on results of previous drilling into the shallow-level plutonic rocks (Leg 147) and extensive regional mapping and sampling surveys, providing a comprehensive geological framework for a composite crustal section. Current knowledge of the Hess Deep crustal sections, in combination with geophysical studies of the EPR, drilling of the plutonic foundation of slow-spreading crust, and studies of ophiolite complexes, allows for the formulation of a series of specific questions that may be tested by drilling at Hess Deep.

Background

Prior to the discovery of axial magma chambers in the late 1980s, general views of the geometry and evolution of the lower crust were dominated by a paradigm derived from studies of gabbroic bodies on land—the layered basic intrusions (Wager and Brown, 1967). These large igneous bodies form in the continental crust as large single magma pulses that crystallize more or less in situ, producing a wide range of magma compositions that can largely be traced to fractional crystallization with minor wall rock assimilation. The oceanic counterpart to these is the "infinite onion" model (Cann, 1974), whereby a single magma body with the approximate depth of the plu-

tonic layer served as a reservoir for magmas, a source for the magmatic cumulates of the plutonic crust, and a feeder for the overlying sheeted dike complex.

Seismic reflection studies along fast- to intermediate-spreading ridges have dramatically changed our view of axial magma chambers (AMCs), revealing melt lenses <1 to 2 km below the seafloor that are ~1 km wide and a few tens of meters thick (Detrick et al., 1987; Hooft et al., 1997; Kent et al., 1990; Singh, 1998). The region underlying the AMCs is a low-velocity zone interpreted to be partially molten, containing <20% melt (e.g., Dunn et al., 2000). The internal structure of this region, such as the distribution of melt and its geometry, is not well constrained because, for example, of the uncertainties of estimating varying melt distribution. Locally, melt has been shown to pool at or below the Mohorovicic discontinuity (Moho), both on- and off-axis, and also within the lower crust off-axis (Garmany, 1989; Crawford and Webb, 2002; Durant and Toomey, 2009; Canales et al., 2009).

Two end-member models for crustal accretion have emerged from geophysical observations along fast-spreading ridges (see above) and geological evidence derived from the Oman and other ophiolites (e.g., Nicolas et al., 1988) (Fig. **F2**). In the gabbro glacier model (Henstock et al., 1993; Quick and Denlinger, 1993; Phipps Morgan and Chen, 1993), most crystallization occurs within a shallow melt lens and the resulting crystal mush subsides downward and outward by crystal sliding to generate the full thickness of the plutonic layer (Fig. **F2A**). The latent heat of the plutonic crust is largely lost to the overlying hydrothermal system on-axis. The sheeted sill model (Kelemen et al., 1997; Korenga and Kelemen, 1997, 1998; MacLeod and Yaouancq, 2000) predicts that almost all of the lower crust crystallizes in situ in a sheeted sill complex, such that melts pond repeatedly as they are transported through the lower crust, with crystallization occurring from the Moho to the AMC (Fig. **F2B**). This requires extensive hydrothermal cooling of the plutonic crust along the sides of the crystal mush zone to remove the latent heat of crystallization on-axis (Chen, 2001). Hybrid models have also been proposed, in which some crystallization occurs in the AMC and some in situ within the plutonic crust (Boudier et al., 1996; Coogan et al., 2002b; Maclennan et al., 2004). In fact, both end-member models require some portion of each process. In the gabbro glacier model, the melt lubricates subsiding crystals, allowing them to flow, would crystallize in the deeper crust. In the sheeted sill model, more rapid cooling at shallower levels in the crust requires some crystal subsidence to prevent the AMC solidifying (e.g., Maclennan et al., 2004).

The compositional framework for the crustal accretion models is largely based on the Oman ophiolite, where there is a significant chemical contrast between upper and lower gabbros (e.g., Pallister and Hobson, 1981; Coogan et al., 2002b). The lava sequence, sheeted dike complex, and upper gabbros have mafic phases and calculated melt compositions that are not consistent with direct derivation from liquids in equilibrium with the upper mantle (as expressed, for example, by their Mg#). In the lower gabbros, compositions are more primitive and range between those of the upper gabbros and melts in equilibrium with the upper mantle.

For comparison, upper gabbros from fast-spreading crust sampled at Hess Deep, Pito Deep, and ODP Site 1256 all show evolved compositions (Hékinian et al., 1993; Perk et al., 2007; Wilson et al., 2006; Koepke et al., 2011). At Pito Deep, however, nearly all the gabbros from >300 m below the base of the sheeted dike complex are much more primitive than at the same structural level at Hess Deep (Hanna, 2004; Perk et al., 2007). This compositional difference suggests that primitive, mantle-derived magma may be transported to shallow depths with little fractionation occurring along the way (Pito Deep) and that crystal fractionation and postcumulus reactions may produce evolved rocks at these depths as well (Hess Deep, Site 1256) (Perk et al., 2007). The new observations at Site 1256 and Pito Deep, in concert with data from Hess Deep, suggest that the competing accretion models may both be viable when spatial and/or temporal variability in magmatic processes along the EPR are considered (Coogan, 2007, in press).

The rate of cooling of the plutonic crust depends on the interplay between the addition of heat by magmatic processes (latent and specific heat of cooling) and heat loss through conductive and hydrothermal convective transport. Several theoretical studies focusing on the axial heat budget have investigated the viability of the lower crustal accretion models (Sleep, 1975; Morton and Sleep, 1985; Chen, 2001; Cherkaoui et al., 2003; Maclennan et al., 2004). Both accretion models, as well as hybrids of the two, have been shown to be viable (e.g., Cherkaoui et al., 2003; Maclennan et al., 2004); however, the lack of observational constraint on key input parameters (e.g., permeability) makes the results of these thermal models uncertain. For a more detailed discussion of the petrochemical and thermal consequences of the competing crustal accretion models, see the review article by Coogan (2007, in press)

Hess Deep Rift crustal section

Geological setting

The Hess Deep Rift is located in the vicinity of the Galapagos triple junction (ridge-ridge-ridge) at the intersection of the Cocos, Nazca, and Pacific plates (Fig. **F3**) (Hey et al., 1972, 1977; Holden and Dietz, 1972). The north-south–trending EPR is spreading at 130 mm/y, and the east-west–trending Cocos-Nazca rift is propagating westward toward the EPR at a rate of 42 mm/y. The major plate boundaries are marked by a series of minor ephemeral rifts to the north and south of the Cocos-Nazca spreading center (Schouten et al., 2008; Smith et al., 2011). These rifts formed in response to the regional stress fields associated with the westward propagation of the Cocos-Nazca spreading center, similar to extension associated with the propagation of a nonerupting dike (Schouten et al., 2008; Floyd et al., 2002). Reconstruction of the bathymetry in this region suggests that the current configuration of the Galapagos triple junction has been active for at least 10 m.y. (Smith et al., 2011). The Galapagos microplate was initiated at ~1.5 Ma. Although the cause is not known, it may be related to the formation of seamounts in the vicinity of Dietz Deep (Fig. **F3**)(Lonsdale, 1989; Smith et al., 2011; Schouten et al., 2008).

The Hess Deep Rift is a complex region that formed by extension in the wake of the westward propagating Cocos-Nazca spreading center. The surface expression of rifting is first evident ~30 km from the EPR, where two 5 km wide, east–west grabens expose ~0.5 Ma crust (Fig. **F4**). As the rift valley traces eastward, the small grabens merge and the rift broadens to ~20 km and deepens to >5400 meters below sea level (mbsl) at Hess Deep. An intrarift ridge rises to 3000 mbsl north of Hess Deep. Further to the east, the tip of the Cocos-Nazca spreading center starts to build a volcanic ridge that spreads at 55 mm/y. Uplifted rift escarpments rise to depths <2200 mbsl to the north and the south of the rift (Northern and Southern Escarpments), and their eastward extension defines the boundaries of the Hess Deep Rift and the "rough/smooth boundary" of the crust produced at the Cocos-Nazca spreading center, known as the Galapagos gore (Holden and Dietz, 1972) (Fig. **F4**).

The western end of the intrarift ridge and its southern slope, described in more detail below, has a coherent distribution of lithologies, with evolved gabbros capping the intrarift ridge and more primitive gabbro along its southern slope toward Hess Deep. Mantle peridotites crop out in the vicinity of Site 895 (Fig. **F4**) and along the western margin of the area surveyed for microbathymetry along the southern slope (Fig. **F5**).

On-bottom seismic and gravity surveys indicate that the western end of the intrarift ridge and its southern slope are underlain by coherent crustal blocks (Ballu et al., 1999; Wiggins et al., 1996). These geophysical results, in combination with the regional geology, has led to a model whereby crustal blocks were unroofed by detachment faulting and block rotation on listric normal faults (Francheteau et al., 1990; Wiggins et al., 1996). This model is supported by structural and paleomagnetic data for ODP Site 894 that indicate that the intrarift ridge represents a large, intact crustal block that has been rotated along both horizontal and vertical axes (MacLeod et al., 1996b; Pariso et al., 1996). MacLeod et al. (1996b) conclude that emplacement of the intrarift ridge was accomplished by a combination of low-angle detachment and high-angle normal faulting. Refinement of this model is in progress, based on new bathymetric data collected as part of a site survey cruise for Expedition 345 (C. MacLeod, unpubl. data, 2008), that considers the role of dynamic uplift associated with the Cocos-Nazca spreading center (MacLeod et al., 2008) and gravitational collapse linked with rifting (Ferrini et al., unpubl. data). An earlier model, that calls for diapiric uplift of serpentinized mantle beneath the intrarift ridge uplift (Francheteau et al., 1990), has largely been abandoned.

The EPR at the latitude of the Hess Deep Rift is made up of many short first-order segments, separated by second-order overlapping spreading centers (Lonsdale 1988). Thus, the crust exposed at the Hess Deep Rift likely formed within a short segment, perhaps at a segment end (Lonsdale 1988). Reconstructions of the EPR flanks indicate several episodes of migrating offsets in the recent past and suggest that the crust now exposed in the Hess Deep Rift formed on the western margin of the EPR (Lonsdale, 1989; Smith et al., 2011; Mitchell et al., 2011). Multichannel seismic reflection profiling along the EPR flanks north of the Northern Escarpment indicates a crustal thickness of 5–5.5 km, with a seismic Layer 3 thickness of 3.0–3.5 km (Zonenshain et al., 1980).

Hess Deep Rift crustal section

The Hess Deep Rift exposes contiguous sections of the mid- to upper crust along the northern and southern bounding escarpments and sections of the mid- to lower crust along the rift valley floor. Extensive investigation of these crustal sections during three submersible cruises (Francheteau et al., 1992; Karson et al., 1992, 2002), a remotely operated vehicle (ROV) cruise (MacLeod et al., unpubl. cruise report, 2008), and Leg 147 (Gillis, Mével, Allan, et al., 1993), makes the Hess Deep Rift the best-studied tectonic window into fast-spreading crust. The geological relationships observed

in the field, coupled with investigations of recovered samples, provide a comprehensive framework for the igneous, metamorphic, and tectonic processes active at the fast-spreading EPR. This geological framework is summarized below by lithologic unit and location; the reader is referred to the cited articles for more in depth review of our state of understanding of this region.

Upper crust

EPR upper crustal sections have been extensively studied along the northern rift escarpment ~29 km northeast of the intrarift ridge and, to a lesser degree, the escarpment south of Hess Deep (Fig. **F4**) (Francheteau et al., 1990; Karson et al., 1992, 2002). Lateral variation in the thickness and internal structure of the volcanic sequence and sheeted dike complex is attributed to temporal variations in magma supply (Karson et al., 2002). The lavas and dikes are normal depleted mid-ocean-ridge basalt (N-MORB) and fall into two compositional groups (Stewart et al., 2002). The main compositional group, which includes most of the dikes and some lavas, has Mg# = 52–66 [Mg# = Mg/(Mg + Fe) × 100]. Significant variations in the major and trace element concentrations and ratios of the dikes, on a scale of meters to kilometers, is interpreted to reflect the intercalation of dikes emanating from distinct magma reservoirs and transported along axis. A low-Fe group composed largely of lavas is attributed to the accumulation of plagioclase that acted to decrease magma bulk density and may enhance eruption potential, thus leading to the dominance of lavas in the low-Fe group (Stewart et al., 2005).

Hydrothermal alteration of the upper crust is largely focused in the sheeted dike complex, where the dikes are variably altered to amphibole-dominated or, locally, chlorite-dominated assemblages (Gillis, 1995; Gillis et al., 2001). No systematic variations are apparent in alteration assemblages or peak metamorphic temperatures with depth, similar to other sheeted dike sections (ODP Holes 504B [Alt et al., 1996] and 1256D [Alt et al., 2010]; Pito Deep [Heft et al., 2008]). The average minimum fluid/rock ratio and fluid flux for the sheeted dike complex, calculated by mass balance using whole-rock Sr isotope compositions, are 0.7×10^6 and 1.5×10^6 kg/m^2, respectively (Gillis et al., 2005), within the range for sheeted dike complexes from other fast- and intermediate-spreading ridges (Barker et al., 2008; Teagle et al., 2003).

Mid- to lower crust

EPR mid- to lower crust has been mapped and studied in three areas: the Northern Escarpment, subjacent to the sheeted dike complex described above; the western end

of the intrarift ridge, including core recovered at Site 894; and the southern slope of the intrarift ridge between 4400 and 5400 mbsl (Fig. **F4**). The general characteristics of the plutonic and associated rocks for each of these areas is described, followed by a summary.

Northern Escarpment

Along the northern rift escarpment, the sheeted dike–plutonic transition is generally marked by a narrow zone of intercalated dikes and gabbros, indicative of a gradational boundary (Karson et al., 2002). In one location, the presence of thermally metamorphosed dikes suggests that locally the gabbros intruded into the base of the sheeted dike complex (Gillis, 2008). The plutonic sequence is dominated by gabbronorite, with lesser amounts of Fe-Ti oxide and amphibole gabbro, varitextured gabbro, olivine gabbronorite, Fe-Ti oxide gabbronorite, and rare tonalite (Hanna, 2004; Kirchner and Gillis, in press; Natland and Dick, 1996). Where the exposed plutonic sequence is thickest (~1000 m), a 150–200 m thick gabbro unit directly underlies the sheeted dike complex and overlies a >500 m thick gabbronorite unit. Elsewhere along the northern rift valley wall where plutonic exposures are much thinner (<140 m), the sheeted dike complex is directly underlain by either gabbronorite or gabbro.

The upper plutonic sequence has a wide range in Mg# (mean Mg# = 0.56; range = 0.76–0.30), with gabbronorite being the most primitive and Fe-Ti oxide ± amphibole gabbro being the most evolved end members (Hanna, 2004; Kirchner and Gillis, in press; Natland and Dick, 1996). The more evolved samples (Mg# < 0.6) are generally concentrated in the upper gabbro unit, with isolated samples within the underlying gabbronorite unit. In general, plutonic rocks from the Northern Escarpment are more evolved than those recovered from the intrarift ridge and Site 894 (Coogan et al., 2002a; Hékinian et al., 1993; Pedersen et al., 1996). Plagioclase displays extensive zoning and a large range in composition ($An_{35–70}$), and the Mg# of mafic phases is similarly broad (orthopyroxene Mg# = 56–68, and clinopyroxene Mg# = 30–80) (Gillis, 1995; Hanna, 2004). Geochemical evidence from magmatic amphibole (e.g., Cl content) hosted in the evolved gabbros, and whole rock Sr isotope compositions of relatively fresh gabbros (Kirchner and Gillis, in press), indicate that hydrothermally altered dikes were assimilated along the sheeted dike–plutonic transition, with the geochemical effects of assimilation reaching depths of at least 800 m into the gabbroic sequence (Gillis et al., 2003). Crystal-plastic deformation in the gabbroic sequence is rare, and weak to strong magmatic foliation is defined by the preferred orientation of plagioclase laths (Coogan et al., 2002a).

Gabbroic samples are variably altered by pervasive fluid flow along fracture networks to amphibole-dominated assemblages. The gabbroic rocks are significantly less altered (average = 11% hydrous phases) than the overlying sheeted dike complex (average = 24%), and the percentage of hydrous alteration diminishes with depth (Gillis, 1995; Kirchner and Gillis, in press). Incipient, pervasive fluid flow along microfractures occurred at amphibolite facies conditions (average temperature = 720°C), with slightly higher temperatures in the lower 500 m of the section (Coogan et al., 2002a; Kirchner and Gillis, in press; Manning et al., 1996). Fluid flow at lower temperatures leads to localized groundmass replacement by greenschist assemblages, as gabbroic outcrops display only minimal brittle deformation (Karson et al., 2002). Lower temperature alteration associated with tectonic unroofing is minimal and is manifest largely as oxidation halos and rare occurrences of clay minerals in the groundmass filling fractures.

Summit of intrarift ridge

Exposures of plutonic rocks at the summit of the western end of the intrarift ridge are located very near the sheeted dike–gabbro transition. This interpretation is based upon

1. The presence of dolerites with EPR compositions and regular north to north-northwest-trending, steeply westward-dipping joint patterns, interpreted as sheeted dike margins, intermixed with gabbroic rocks along the northern margin of the intrarift ridge (MacLeod et al., 2008);
2. The compositional overlap with the gabbroic sequence that underlies the sheeted dike complex exposed along the Northern Escarpment (Natland and Dick, 1996; Pedersen et al., 1996; Coogan et al., 2002a); and
3. Cooling rates comparable to the uppermost gabbros at the Northern Escarpment and Oman ophiolite (Faak et al., 2011; Coogan et al., 2007a).

The summit of the western end of the intrarift ridge is largely composed of olivine gabbro, gabbronorite, oxide gabbronorite, gabbro, and patches of pegmatitic amphibole gabbro (Fig. **F6**). These upper gabbroic rocks lack modal layering but locally contain lithologic boundaries identified by grain-size variation (Gillis, Mével, Allan, et al., 1993; Hékinian et al., 1993). The most chemically evolved gabbroic rocks (Mg# mean = 0.58; range = 0.35–0.68) are found along the northern margin of the intrarift ridge, north of proposed Site HD-04B and Site 894 (Fig. **F7**). The compositional range is slightly narrower at Hole 894G (Mg# mean = 0.65; range = 0.51–0.68) and becomes slightly more mafic along the slope immediately south of the summit (mean Mg# =

0.74; range = 0.65–0.85). Similar to the Northern Escarpment, plagioclase displays extensive zoning and a large range in composition ($An_{44–87}$), whereas the range of Mg # for mafic phases is less broad (olivine $Fo_{61–71}$, orthopyroxene Mg# = 64–74, and clinopyroxene Mg# = 62–81) (Pedersen et al., 1996; Natland and Dick, 1996; Kelley and Malpas, 1996).

The gabbroic rocks at Site 894 show no systematic variation in mineral or bulk rock compositions downhole but exhibit small-scale (1–5 m) excursions in elemental abundances (Natland and Dick, 1996; Pedersen et al., 1996). The parental melts are highly depleted (Pedersen et al., 1996), consistent with the refractory harzburgites recovered at Site 895 (Dick and Natland, 1996; Arai et al., 1997). Strongly zoned plagioclases and unusually high Cr contents of clinopyroxenes indicate early crystallization from a primitive magma (Natland and Dick, 1996). Local enrichment in incompatible elements in rocks that are relatively enriched in compatible elements indicates interactions of a partly crystallized matrix with a high abundance of interstitial melt (Pedersen et al., 1996). Alternatively, using a different geochemical approach that invokes a more evolved parental magma, Natland and Dick (1996) predict that a partly crystallized matrix interacted with very low abundances of interstitial melt.

Crystal-plastic deformation is rare in the gabbroic rocks at the summit of the intrarift ridge, with minor undulose extinction and very rare deformation twins in plagioclase. Similar to the Northern Escarpment gabbroic rocks, weak to strong magmatic foliation is defined by the preferred orientation of plagioclase laths (Hékinian et al., 1993; Coogan et al., 2002a; Gillis, Mével, Allan, et al., 1993; MacLeod et al., 1996a). Reorientation of some sections of the Hole 894G core to geographical coordinates shows that the foliations are steeply dipping (mean dip = 69°) with a nearly north–south orientation, parallel to the EPR, and that there is steeply plunging lineation (MacLeod et al., 1996a). Measurements of the anisotropy of magnetic susceptibility in samples show that there is also a magnetic fabric parallel to the plagioclase fabric (Richter et al., 1996).

Similar to the upper gabbroic sequence at the Northern Escarpment, incipient fluid flow was initiated along microfractures at high temperatures (Manning et al., 1996; Manning and MacLeod, 1996). When this upper gabbroic section had cooled to a temperature of ~450°C, it became influenced by the effects of Cocos-Nazca rifting, creating a dense array of east–west tensile fractures filled with greenschist to zeolite facies assemblages (Früh-Green et al., 1996; Manning and MacLeod, 1996). Away from the late-stage brittle fractures, gabbroic rocks are variably altered to amphibole-

dominated assemblages (Früh-Green et al., 1996). Whole-rock samples unaffected by this lower temperature stage of brittle deformation are depleted in $\delta^{18}O$ relative to fresh values (Agrinier et al., 1995; Lécuyer and Reynard, 1996) and show minor enrichment in $^{87}Sr/^{86}Sr$ (Lécuyer and Grau, 1996). Calculated fluid/rock ratios using both isotopic systems range from 0.1 to 1 (Lécuyer and Grau, 1996; Lécuyer and Reynard, 1996).

Mantle peridotites are exposed in the vicinity of Site 895, southeast of Site 894 (Fig. **F4**). Clinopyroxene-poor harzburgites, at the most depleted end of the range for abyssal peridotites, are interpreted to be the residues of melting of an N-MORB source (Dick and Natland, 1996). The association of dunite-troctolite-olivine gabbro with depleted harzburgite records the interaction of migrating melt with depleted harzburgite wall rock in the shallowest mantle (Dick and Natland, 1996; Arai and Matsukage, 1996; Arai et al., 1997). The geometry of these associations suggests that at least some melt transport was fracture controlled. Significant modal layering in the gabbroic rocks, a feature of the Oman mantle transition zone (Korenga and Kelemen, 1997), was not observed.

Lower slope of intrarift ridge

Plutonic rocks dominate the central and eastern region of the southern slope of the intrarift ridge, between 4400 and 5400 mbsl (Fig. **F5**). Plutonic rocks range in composition with gabbros, gabbronorites, and olivine gabbros that are, on average, more primitive than the summit of the intrarift ridge (mean Mg# = 0.71; range 0.39–0.85) (Fig. **F7**) (Blum, 1991; C. MacLeod, unpubl. data, 2009). Plagioclase is less zoned and on average is more anorthitic, and the Mg# of mafic phases have a more restricted range than the upper gabbros (plagioclase $An_{87–48}$; olivine $Fo_{72–88}$, orthopyroxene Mg# = 67–88, and clinopyroxene Mg# = 65–89) (Hékinian et al., 1993). Unlike shallower level gabbros, the Mg# and compatible elements in olivine and clinopyroxene covary, such that decreases in Mg# and compatible elements in the melts and rapid decreases in the most compatible elements can be largely explained by fractional crystallization processes (Coogan et al., 2002a; Hékinian et al., 1993). Layering was locally observed in outcrop, and many samples display weak to strong magmatic foliation.

Similar to the upper gabbroic sequence, incipient fluid flow was initiated along microfractures at high temperatures (Agrinier et al., 1995; Coogan et al., 2002a) and was later influenced by lower temperature hydrothermal alteration associated with Cocos-Nazca rifting (Agrinier et al., 1995).

Basaltic rocks associated with the intrarift ridge

Basaltic rocks, distributed throughout the intrarift ridge (labeled dolerite and basalt in Fig. F5), have two possible origins: (1) the EPR or (2) more recent intrusion of Cocos-Nazca magmas into rifted EPR crust, in advance of full Cocos-Nazca spreading. Although unequivocal chemical criteria to distinguish between EPR and Cocos-Nazca spreading center origin have not yet been established, basaltic samples that are more depleted in incompatible trace elements than EPR basalts recovered along the Northern Escarpment of the Hess Deep Rift (Stewart et al., 2002) or the equatorial EPR (Petrological Database of the Ocean Floor, www.petdb.org/) are commonly attributed to the Cocos-Nazca spreading center.

At the summit of the intrarift ridge, basaltic rocks along the northern margin of the intrarift ridge have EPR compositions and regular north- to north-northwest-trending, steeply westward-dipping joint patterns indicative of a sheeted dike complex (MacLeod et al., 2008). Rare basaltic dikes recovered from Hole 894G have more equivocal origins, being interpreted as originating at the EPR (Pedersen et al., 1996) or from a Cocos-Nazca spreading center source (Allan et al., 1996).

Along the southern slope of the intrarift ridge, basaltic rocks dominate between 4000 and 4400 mbsl, are intermixed with gabbroic rocks and peridotites in the central and eastern regions between 4400 and 5400 mbsl, and dominate in the western region between 4400 and 5400 mbsl (note that the western region lacks comprehensive coverage) (Fig. F5). The majority of the basaltic rocks (60%) have compositions that fall within the range of EPR sheeted dikes and lavas exposed along the northern rift valley wall (Stewart et al., 2002; Hékinian et al., 1993). The remaining samples are generally more depleted and primitive than the EPR dikes and lavas and thus may be associated with Cocos-Nazca rifting.

Summary

It is not possible to place the southern slope of the intrarift ridge into a precise structural context, as the nature of intermediate to lower plutonic crust formed at fast-spreading ridges is largely unknown. What we know very clearly is that the primitive gabbros structurally underlie regions where evolved gabbros dominate at the Hess Deep Rift. The geological relationships along the Northern Escarpment provide the best evidence for this, as evolved gabbros dominate the entire 800 m of the gabbro exposures that extend downward from the base of the sheeted dike complex. In this

way, the southern slope of the intrarift ridge between 4400 and 5400 mbsl is likely analogous to the intermediate to lower plutonic rocks of the Oman ophiolite.

Gabbroic rocks from the Hess Deep Rift have a broad range in composition, from primitive troctolites to evolved Fe-Ti ± amphibole gabbros. In general, the plutonic sequence is dominated by cumulates, with the lower gabbros being more primitive and less enriched in incompatible elements than the upper gabbros. The nature of mantle-crossing melts and their evolution within the crust is still being debated. The geochemical trends constrained to date, from the Moho to the base of the sheeted dike complex, suggest the plutonic crust is built by fractional crystallization from primitive melts, with greater amounts of reaction with interstitial melt in the upper plutonics or crystallization of the upper plutonics from highly fractioned melts.

Gabbros from the Hess Deep Rift provide the first constraints on fracture formation and metamorphism in the root zones of hydrothermal systems at the EPR. Seawater influx into Layer 3 commenced soon after crystallization, with pervasive influx of water along randomly oriented microfracture networks and grain boundaries, mostly at temperatures of 600°–750°C. This permeability was probably created by tensile brittle failure upon subsolidus cooling and thermal contraction of the gabbro. When the upper plutonic section had cooled to a temperature of ~450°C, it became influenced by the effects of Cocos-Nazca rifting, and a dense array of east-west tensile fractures developed.

Scientific objectives

The principal objective for drilling at the Hess Deep Rift is to test competing hypotheses of magmatic accretion and hydrothermal processes in the lower ocean crust formed at the fast-spreading EPR. These hypotheses make predictions that can only be tested with drill cores, including the presence or absence of systematic variations in mineral and bulk rock compositions, presence or absence of modally layered gabbro, and the extent and nature of hydrothermal alteration and deformation. Specific scientific questions that address these predictions are outlined below.

How is melt transported from the mantle through the lower crust?

Melts erupting at mid-ocean ridges are almost never saturated in all mantle phases at plausible segregation depths (O'Hara, 1968; Stolper and Walker, 1980). The upper

mantle and crustal processes responsible for the evolution of mantle primary melts into primitive MORB are the subject of a great many studies in the geochemical literature (e.g., Kelemen et al., 1997). Melts are transported and aggregated by porous flow at both mantle and crustal levels; the latter is a process that may be identified on the basis of textural and chemical evidence. The different mechanisms of igneous differentiation (e.g., fractional crystallization, equilibrium crystallization, assimilation, and porous reactive flow) strongly influence the chemical evolution of residual liquids and host cumulates. Melt transport through the lower crust is an important boundary condition of the crustal accretion models. Is melt transported largely via porous flow through the lower crust, or is it transported in dikelike brittle fractures (Kelemen and Aharanov, 1998)? Mineral and bulk chemical data for the core will provide tests for both the mechanisms of igneous differentiation and melt transport in the base of the ocean crust.

What is the origin and significance of layering?

Modally and compositionally layered gabbroic rocks are common in the lower crustal sections of ophiolites (e.g., Anonymous, 1972). A layered lower crust is thus one of the key and nearly ubiquitous features of all models of the fast-spreading lower crust. However, modal layering of the sort observed in major ophiolites has rarely been observed or sampled on the ocean floor so far. This may be because commonly used sampling and observation methods are not ideal to detect such layering readily, the right areas have not been sampled, or the layering is absent. If ophiolites indeed represent sections of normal mid-ocean-ridge crust, we expect to drill significant thicknesses of layered igneous rocks in this expedition. Their nature and extent is likely to have a strong bearing on the applicability of ophiolite-based accretionary models for the formation of the lower ocean crust.

How, and how fast, is heat extracted from the lower plutonic crust?

Hydrothermal fluids initially penetrate all levels of the plutonic crust along microfracture networks at high temperatures, with fractures sealing at 600°–800°C (Alt et al., 2010; Manning et al., 1996; Coogan et al., 2002a). Initiation of incipient cracking in the upper gabbros at Hess Deep overlaps the solidus temperatures of the most evolved lithologies, as recorded in magmatic amphibole (850°–925°C) (Gillis et al., 2003) and zircon (690°–790°C) (Coogan and Hinton, 2006). Whether this is the case in the lower plutonic crust, where more primitive lithologies dominate, is not known. Penetration of fluids at high enough temperatures could promote hydrous partial

melting (Koepke et al., 2007); if and at what depth this process occurs is not known. Cooling rates for upper gabbro sections from fast-spreading crust and equivalent sections from the Oman ophiolite are rapid (4000°–5000°C/m.y.) (Coogan et al., 2002b, 2007a), indicative of significant convective cooling. Slower cooling rates in the Oman ophiolite suggest that heat flow was largely conductive (Coogan et al., 2002b, 2007a), cooling rates for lower gabbro sections from fast-spreading crust are not known.

Coring will allow us to determine the thermal history of the lower plutonic rocks using recently developed geospeedometric and thermometric methods. Temperature-time paths may be constructed by dating minerals with different thermal histories (e.g., John et al., 2004) and cooling rates may be calculated using Ca-in-olivine, Li-in-plagioclase, and other developing geospeedometers that quantify the diffusive exchange of elements between minerals (e.g., Coogan et al., 2005, 2007a). Using these and other approaches, it will be possible to determine the timing and rate of hydrothermal cooling in the lower plutonics, addressing questions such as, What is the rate of cooling with depth? Is hydrothermal flow along microfracture networks an effective mechanism to cool the lower crust? When is hydrothermal cooling initiated? Does fluid penetration occur at high enough temperatures to induce hydrous partial melting? Does the lower crust cool largely by conductive or convective heat transport?

What are the fluid and geochemical fluxes in the EPR lower plutonic crust?

Our understanding of the extent of fluid flow and reaction in the lower crust is presently very limited. Thermal models developed to test the crustal accretion models predict that advective cooling of the lower plutonic crust at or very close to the EPR would lead to a progressive decrease in the fluid flux and attendant fluid-rock interaction with depth, whereas more gradational conductive cooling over a broader time frame would likely lead to lower fluid fluxes and more limited fluid-rock interaction. Bulk rock Sr isotope data have constrained the time-integrated fluid fluxes for the upper crust (Bickle and Teagle, 1992; Gillis et al., 2005; Teagle et al., 2003; Kirchner and Gillis, in press); application of this approach will allow us to constrain fluid fluxes in the lower crust. Thermodynamic modeling predicts that high-temperature fluid flow and reaction would leave little macroscopic evidence (McCollum and Shock, 1998), which is supported by $\delta^{18}O$ data for petrologically fresh samples (Alt and Bach, 2006; Gao et al., 2006). Thus, it will be critical to combine petrological and geochemical data to assess the extent of fluid-rock interaction in the lowermost plutonic crust.

Well-established petrological and geochemical techniques may be used to characterize the extent, nature, and timing of chemical exchange between the lower plutonic crust and seawater. Stable isotope compositions of minerals and geothermometers may be used to determine the temperature of hydrothermal replacement (e.g., Alt et al., 2010; Früh-Green et al., 1996; Manning et al., 1996). Major and trace elements and stable and radiogenic isotope compositions of minerals and whole rocks will provide constraints on the chemical evolution of fluid compositions and their origin (e.g., seawater-derived versus magmatic fluids) (e.g., Gregory and Taylor, 1981; Teagle et al., 1998; Gillis et al., 2003). Using these and other approaches, it will be possible to address questions, such as, How does the extent of alteration vary with depth? How does fluid flux vary with depth? What is the extent of chemical exchange between the lower crust and seawater? At what temperature is fluid-rock interaction initiated? What is the role of magmatic fluids?

In order to address the questions listed above, it will be important to distinguish between structures and hydrothermal alteration that formed at and near the EPR versus those associated with Cocos-Nazca rifting. This may be achieved by using standard petrographic techniques, in combination with Formation MicroScanner and structural data, as was done successfully on cores from Hole 894G (e.g., MacLeod et al., 1996b).

Drilling strategy and operations plan

The highest priority for drilling at Hess Deep will be to sample one or more 100 to ≥250 m long sections of primitive gabbroic rocks. Three primary drill sites have been identified; however, if coring is proceeding well in the first or second of these sites, it will be continued as long as possible in order to capitalize on good drilling conditions and obtain the longest possible continuous sample.

The primary drill sites (proposed Sites HD-01B, HD-02B, and HD-03B) are situated on a flat-lying, east–west-trending, sedimented bench at ~4850 mbsl along the southern slope between the intrarift ridge and Hess Deep, in an area dominated by primitive gabbros (Figs. **F5, F8**). A ~200 m wide, flat-lying bench is covered with ~15 m of pelagic sediment mixed with lithic debris. The slope north of the bench is the footwall of a steeply dipping, southward-facing normal fault. The bench itself has a series of 5–15 m high, northward-striking narrow ridges that are attributed to the combined effects of variation in sediment thickness, sediment draping over small-scale basement structures, and/or relief caused by westward-dipping, northward-striking nor-

mal faults. The three drill sites are carefully located to be as far removed from these surface features as possible and to maximize the lengths of unfaulted sections that we will drill. The drill holes should encounter contiguous vertical sections on the order of 90–290 m in the footwall (Fig. **F5**). Our drill sites are spaced from 300 to 400 m apart along the bench to maximize coverage of the area where primitive gabbros (Mg# = 75–85) crop out within 150–200 m to the north and south (see distribution of olivine gabbros in Figs. **F5, F8**). As described above, an east–west transect is not intended, rather drilling will proceed at one or more sites as long as possible. In case drilling conditions at these sites prove impossible, we are requesting permission to relocate sites anywhere on the bench. These strategies are intended to maximize our chances of meeting our principal scientific objectives, which are to determine how melt is transported from the mantle through the crust, where melts fractionate and crystallize, and the extent and nature of hydrothermal alteration and deformation.

Alternate proposed Site HD-04B is located a few hundred meters north of Hole 894G, at the summit of the western end of the intrarift ridge (Figs. **F4, F6**). The summit is covered by <10 m of flat-lying pelagic ooze mixed with lithic debris (Gillis, Mével, Allan, et al., 1993). At alternate proposed Site HD-04B, a borehole would start in evolved upper gabbros but there is potential of recovering more primitive lithologies at several hundred meters depth because the gabbroic rocks become more mafic along the slope of the intrarift ridge immediately to the south.

Operations plan

Although we present an example operations plan in Table **T1,** the single primary goal of our expedition is to establish a hole that can be reentered multiple times, allow formation stability to be maintained, and core/log that hole as deeply as possible. When this occurs, all remaining available time may be spent on this hole and other holes/sites will not be established.

We anticipate that drilling, coring, and logging operations in the Hess Deep Rift may be quite challenging. We are preparing a range of potential operational approaches that we might apply to address challenges that include very thin sediment cover, initiating/maintaining a hole through the basement contact, and coring deeply through potentially unstable basement.

Given all this, it is unlikely that the expedition operations will unfold as presented in Table **T1.**

Operational approach(es)

To maximize the potential to achieve the operational and scientific objectives of initiating and advancing a deep hole, we plan to provide the hardware and supplies to implement a variety of operational approaches. Maintaining maximum operational flexibility will provide the highest chance of success in this challenging environment. There are many combinations and permutations of operational scenarios possible which will continue to be evaluated leading up to the expedition and will all be under consideration as the expedition progresses. Sediment thickness, nature of upper basement drilling/coring conditions, and hole stability will determine which approach may be the most viable. The operational scenarios can basically be categorized into four general approaches depending upon the actual conditions encountered. At each site, a series of pilot holes will be drilled/cored to verify formation conditions.

Standard reentry cone approach

Deployment of a standard reentry cone is the most favored operational approach. This approach is shown in Figure **F9** and Table **T1.** If successful, this approach allows the best chance of success at achieving the deeper objectives because it allows the best chance to combat anticipated unstable hole conditions and provides a possible opportunity to case off upper basement formation if required. This approach starts with jetting in a standard reentry cone with a short section of 20 inch casing. Then an 18.5 inch hole is drilled into uppermost basement into which 16 inch casing is installed and cemented. Rotary core barrel (RCB) coring and logging would extend below the base of the casing. If necessary to stabilize the hole, a third casing string (10.75 inch) may also be deployed. The thinnest sediment cover in which a standard reentry cone has been successfully deployed is ~38 m during Expedition 336. Attempting to do this in less sediment, as expected at the drill sites, may be problematic (see below). One concern is possible undermining of the reentry cone base plate from drilling circulation while drilling the 18.5 inch hole into basement.

Free-fall funnel approach

Another possible operational option is to deploy a free-fall funnel (FFF) or "nested" FFFs in an attempt to facilitate multiple reentries of an existing hole. There is a spectrum of possible operational options that entail using FFF or "modified" FFF technology. A couple of potential options are shown in Figure **F10.** This approach may take a bit less operational time to deploy than a standard reentry cone; however, it does not provide an option to deploy casing to stabilize any unstable basement below nor

does it provide as robust a seafloor structure to remediate an unstable hole or problematic drilling conditions. Historically there can be problems with FFFs being pulled out of the hole when pulling the core bit out of the hole. FFFs also can occasionally interfere with reentering the basement portion of the hole because of washing of the sediment overlying the basement contact and offsetting of the bottom of the FFF casing from the hole in basement. One potential way to address this would be to cement the FFF into the basement as shown in Figure **F10.**

Bare rock reentry approach

This operation would be to rely on the ability make multiple reentries into small diameter (10–20 inch) bare rock holes without installation of a seafloor structure. This is shown in Figure **F11.** Once again, this approach has many potential operational combinations and permutations. This approach is likely to be the quickest at getting to RCB coring and could be attempted at any of the pilot holes. Although bare rock reentries have been successful in the past, this approach will likely require the most amount of time for subsequent reentries; is more impacted by changes in environment such as variable current, changing sea states, and so on; and is the least capable of supporting remedial actions caused by unstable hole problems. A larger diameter hole near the surface to facilitate reentry and potentially accommodate subsequent seafloor structure installation could also be made with an underreamer or bi-center reamer positioned above the main bit (e.g., create a countersunk hole; Figure **F11,** scenario 3); however, its likely that no coring can be undertaken when running these reamers.

Bare rock installation of a reentry cone with short casing pup

This scenario would allow a cased hole on bare or thinly sedimented rock (<10 m). After a large-diameter hole is drilled a few meters into basement, a short section of casing with casing hanger and reentry cone is lowered into the hole. The hole then would be able to be continued deeper with casing as described above (see **"Standard reentry cone approach"**). However, lowering such a seafloor structure into the hole is probably not possible with the standard camera system, which cannot see around and below the reentry cone. This likely would require a through-pipe camera, which is not part of the normal operational equipment available.

Tentative planned sequence of operations

1. Locate site per coordinates provided, deploy camera/sonar system, and conduct limited seafloor survey to confirm acceptability of proposed drilling area.

2. Conduct a series of probes into the seafloor to basement at multiple locations to determine approximate variation in sediment thickness and estimate slope of seafloor and basement contact. This can be done by "jetting" the drill string through the sediment until the basement contact is reached. This should be a fairly rapid operation given the drill string only has to be pulled clear of the seafloor between probes and the camera can remain deployed.
3. Based upon the camera survey, probe information, and other available data, identify a location to attempt drilling a pilot hole.
4. Spud and deepen a pilot hole 50–100 m into basement using the RCB. Ultimate depth of the pilot hole will be determined by hole stability, core recovery, and science evaluation of the core data. Note that multiple pilot holes may be required before a suitable drilling location is identified.
5. Based on pilot hole drilling conditions, three options are suggested:
    a. If the pilot hole is going well and there is reasonable belief that the hole can be successfully deepened and valuable core data obtained, then the coring operation should be terminated based upon a "conservative" estimate of rotating bit hours (40–45 h) and the drill string round-tripped for a bit change. A FFF can be deployed prior to clearing the seafloor, or plans can be made to reenter the bare rock hole with a second RCB core bit.
    b. If the pilot hole determines that this location is not suitable for attempting to achieve the scientific objectives, then the area can be abandoned and another location selected for evaluation.
    c. If the pilot hole is not considered suitable for deepening but the location is considered adequate for an attempted deeper "reentry" hole, then the operational approaches identified above can be discussed and an operational approach decided upon using the hardware and personnel resources available onboard.

Recent improvements in drilling unstable hard rock formations

Several improvements in drilling/coring fractured hard rock formations have been made recently. We now use "blended" cement made up of standard American Petroleum Institute (API) Class G cement blended with 0.25 lb of Cello Flake lost circulation material (LCM) per 94 lb sack of cement. We have had much better success cementing casing in fractured formations using this blended cement.

Standard API Class G cement has also recently been used successfully during Expedition 335 to cement problematic zones within a borehole, allowing further successful advancement of the hole.

Also, we have determined that significantly larger mud sweeps are required to achieve adequate hole cleaning in these environments. In the past, typical mud sweeps ranged from 15 to 25 bbl. Recently, during Expedition 327 (Juan de Fuca), mud sweeps in excess of 100 bbl were used with good success.

Finally, in the past there was concern that "working" a hole too much could in effect do more damage than good. Whereas this is always a possibility, we have found that in many cases tenacity and multiple wiper trips actually eventually paid dividends in cleaning up the hole and allowing successful advancement.

All of these improvements will be kept in mind as we tackle the challenges of successful drilling/coring operations in the Hess Deep environment.

Operational challenges

Drilling and coring operations are anticipated to be challenging during the Hess Deep expedition. Water depths in excess of 4400 m will impact routine operations such as pipe tripping, reentry, and wireline coring/logging, making these operations more time consuming than they would be in shallower water. Because of the anticipated limited sediment cover on location, the installation of a reentry structure may be more problematic than normal. Following installation of a reentry system, basement drilling/coring operations are expected to be difficult, with unstable hole conditions and difficulty performing effective hole cleaning. If a sustainable hole is achieved and deepened, core recovery in basement is typically fairly low and deployment of wireline logging tools may not be possible in unstable holes. Despite these challenges, the ultimate operational goal is to establish a hole capable of sustaining multiple reentries (allowing multiple bit changes), with "adequate" hole stability, deepen that hole as far as possible with continuous RCB coring, and recover a full suite of wireline logs.

Wireline logging

Wireline logs will be recorded at every site to measure the in situ physical properties of the formation and to complement the incomplete core recovery that is typical of basement drilling and expected in this challenging drilling environment. These data

will help define the thickness of lithologic units, characterize alteration patterns, or estimate fracture density. They will also be crucial to characterize the local structure and provide orientation to structural features observed on the cores. The data from the wireline logging will be integrated with measurements on the core in order to pin individual core pieces to a specific wireline depth, to geographically orient the core pieces, and to constrain to the extent possible the characteristics of the uncored intervals.

Two logging strings will be used:

1. The triple combination (triple combo) tool string will include the High Resolution Laterolog Array (HRLA), which measures the resistivity of the formation; the Accelerator Porosity Sonde (APS), which measures porosity; the Hostile Environment Litho-Density Sonde (HLDS), which measures density; and the Hostile Environment Natural Gamma Ray Sonde (HNGS), which measures spectral gamma radiation and the contributions of uranium, thorium, and potassium. The caliper of the HLDS will measure the size of the hole that will allow an assessment of the quality of the data and the hole conditions for the following string.
2. The FMS-sonic tool string is composed of the Dipole Sonic Imager (DSI), which measures sonic velocity, and the FMS, which provides microresistivity images of the borehole wall. As part of the FMS, the General Purpose Inclinometry Tool (GPIT) includes a three-axis accelerometer and a three-axis magnetometer to monitor tool motion and provide orientation for the images of the surrounding structure. In addition to the shear and compressional velocity of the formation, the DSI uses two orthogonal dipole sources to measure acoustic anisotropy that can be used to determine preferred mineral and/or fracture orientations, fracture densities, and stress directions. Stoneley waveforms will also be recorded that could help identify fractures and constrain the permeability around the borehole.

A potential additional logging tool string with the Magnetic Susceptibility Sonde (MSS) and the multisensor Magnetometer Module (MMM) may be available. These two tools are in development and testing is planned prior to Expedition 345. If the tests are successful, these tools will be available for the expedition. If time allows, they could be deployed to investigate the in situ magnetic properties of the crust recovered at Hess Deep.

All of the wireline tools and their applications are described at **iodp.ldeo.columbia.edu/TOOLS_LABS/index.html.**

Research planning: sampling and data sharing strategy

Shipboard and shore-based researchers should refer to the IODP Sample, Data, and Obligations policy posted on the Web at **www.iodp.org/program-policies/.** This document outlines the policy for distributing IODP samples and data to research scientists, curators, and educators. The document also defines the obligations that sample and data recipients incur. The Sample Allocation Committee (SAC; composed of Co-Chief Scientists, Staff Scientist, and IODP Curator on shore and curatorial representative on board ship) will work with the entire scientific party to formulate a formal expedition-specific sampling plan for shipboard and postcruise sampling.

Before the expedition, all shipboard scientists are required to submit research plans and associated sample/data requests at **smcs.iodp.org** before 1 September 2012. Based on sample requests (shore based and shipboard) submitted by this deadline, the SAC will prepare a tentative sampling plan, which will be revised on the ship as dictated by recovery and cruise objectives. For the purpose of developing sample requests, participating scientists should expect to receive 25–100 samples each of no more than ~25 cm^3. These are just guidelines based on historic precedent from ODP and IODP designed to enable scientists to complete a research program and meet the established publication deadlines. In any case, all postcruise research projects should justify scientific reasons for desired sample size, numbers, and frequency. The sampling plan will be subject to modification depending upon the actual material recovered and collaborations that may evolve between scientists during the expedition. Modifications to the sampling strategy during the expedition must be approved by the SAC.

The minimum permanent archive will be the standard archive half of each core. All sample frequencies and sizes must be justified on a scientific basis and will depend on core recovery, the full spectrum of other requests, and the expedition objectives. Some redundancy of measurement is unavoidable, but minimizing the duplication of measurements among the shipboard party and identified shore-based collaborators will be a factor in evaluating sample requests.

If critical intervals are recovered (e.g., mineralization, veins, breccias, dike or glassy margins, thin gabbroic intervals, etc.), there may be considerable demand for samples from a limited amount of cored material. These intervals may require special handling, a higher sampling density, or reduced sample size. A sampling plan coordinated by the SAC may be required before critical intervals are sampled.

We strongly encourage, and may require, collaboration and/or sharing among the shipboard and shore-based scientists so that the best use is made of the recovered core. We anticipate coordination of postcruise analytical programs to ensure that the full range of geochemical, isotopic, magnetic, and physical property studies are undertaken on a representative sample suite. We expect that all sampling will take place on board the ship and encourage scientists to start developing collaborations before and during Expedition 345.

References

Agrinier, P., Hékinian, R., Bideau, D., and Javoy, M., 1995. O and H stable isotope compositions of oceanic crust and upper mantle rocks exposed in the Hess Deep near the Galapagos triple junction. *Earth Planet. Sci. Lett.,* 136(3–4):183–196. **doi:10.1016/0012-821X(95)00159-A**

Allan, J.F., Falloon, T., Pedersen, R.B., Shankar Lakkapragada, B., Natland, J.H., and Malpas, J., 1996. Petrology of selected Leg 147 basaltic lavas and dikes. *In* Mével, C., Gillis, K.M., Allan, J.F., and Meyer, P.S. (Eds.), *Proc. ODP, Sci. Results,* 147: College Station, TX (Ocean Drilling Program), 173–186. **doi:10.2973/odp.proc.sr.147.010.1996**

Alt, J.C., and Bach, W., 2006. Oxygen isotope composition of a section of lower oceanic crust, ODP Hole 735B. *Geochem., Geophys., Geosyst., 7*(12):Q12008. **doi:10.1029/2006GC001385**

Alt, J.C., Laverne, C., Coggon, R.M., Teagle, D.A.H., Banerjee, N.R., Morgan, S., Smith-Duque, C.E., Harris, M., and Galli, L., 2010. Subsurface structure of a submarine hydrothermal system in ocean crust formed at the East Pacific Rise, ODP/IODP Site 1256. *Geochem., Geophys., Geosyst.*, 11:Q10010. **doi:10.1029/2010GC003144**

Alt, J.C., Laverne, C., Vanko, D.A., Tartarotti, P., Teagle, D.A.H., Bach, W., Zuleger, E., Erzinger, J., Honnorez, J., Pezard, P.A., Becker, K., Salisbury, M.H., and Wilkens, R.H., 1996. Hydrothermal alteration of a section of upper oceanic crust in the eastern equatorial Pacific: a synthesis of results from Site 504 (DSDP Legs 69, 70, and 83, and ODP Legs 111, 137, 140, and 148.) *In* Alt, J.C., Kinoshita, H., Stokking, L.B., and Michael, P.J. (Eds.), *Proc. ODP, Sci. Results,* 148: College Station, TX (Ocean Drilling Program), 417–434. **doi:10.2973/odp.proc.sr.148.159.1996**

Anonymous, 1972. Penrose field conference on ophiolites. *Geotimes,* 17:24–25.

Arai, S., and Matsukage, K., 1996. Petrology of gabbro-troctolite-peridotite complex from Hess Deep, equatorial Pacific: implications for mantle-melt interaction within the oceanic lithosphere. *In* Mével, C., Gillis, K.M., Allan, J.F., and Meyer, P.S. (Eds.), *Proc. ODP, Sci. Results,* 147: College Station, TX (Ocean Drilling Program), 135–155. **doi:10.2973/odp.proc.sr.147.008.1996**

Arai, S., Matsukage, K., Isobe, E., and Vysotskiy, S., 1997. Concentration of incompatible elements in oceanic mantle: effect of melt/wall interaction in stagnant or failed melt conduits within peridotite. *Geochim. Cosmochim. Acta,* 61(3):671–675. **doi:10.1016/S0016-7037(96)00389-4**

Ballu, V., Hildebrand, J.A., and Canuteson, E.L., 1999. The density structure associated with oceanic crustal rifting at the Hess Deep: a seafloor and sea-surface gravity study. *Earth Planet. Sci. Lett.,* 171(1):21–34. **doi:10.1016/S0012-821X(99)00132-6**[†]

Barker, A.K., Coogan, L.A., Gillis, K.M., and Weis, D., 2008. Strontium isotope constraints on fluid flow in the sheeted dike complex of fast-spreading crust: pervasive fluid flow at Pito Deep. *Geochem., Geophys., Geosyst.,* 9(6):Q06010. **doi:10.1029/2007GC001901**

Bédard, J.H., Sparks, R.S.J., Renner, R., Cheadle, M.J., and Hallworth, M.A., 1988. Peridotite sills and metasomatic gabbros in the eastern layered series of the Rhum complex. *J. Geol. Soc. (London, U. K.),* 145(2):207–224. **doi:10.1144/gsjgs.145.2.0207**

Bickle, M.J., and Teagle, D.A.H., 1992. Strontium alteration in the Troodos ophiolite: implications for fluid fluxes and geochemical transport in mid-ocean ridge hydrothermal systems. *Earth Planet. Sci. Lett.,* 113(1–2):219–237. **doi:10.1016/0012-821X(92)90221-G**

Blackman, D.K., Ildefonse, B., John, B.E., Ohara, Y., Miller, D.J., MacLeod, C.J., and the Expedition 304/305 Scientists, 2006. *Proc IODP,* 304/305: College Station, TX (Integrated Ocean Drilling Program Management International, Inc.). **doi:10.2204/iodp.proc.304305.2006**

Blum, N., 1991. Structure and composition of oceanic crust and upper mantle exposed in Hess Deep of the Galapagos microplate (equatorial east Pacific) [Ph.D. dissert.]. Univ. Karlsruhe, Germany.

Boudier, F., Nicolas, A., and Ildefonse, B., 1996. Magma chambers in the Oman ophiolite: fed from the top and the bottom. *Earth Planet. Sci. Lett.,* 144(1–2):239–250. **doi:10.1016/0012-821X(96)00167-7**

Canales, J.P., Nedimovic, M.R., Kent, G.M., Carbotte, S.M., and Detrick, R.S., 2009. Seismic reflection images of a near-axis melt sill within the lower crust at the Juan de Fuca Ridge. *Nature (London, U. K.),* 460(7251):89–93. **doi:10.1038/nature08095**

Cann, J.R., 1974. A model for oceanic crystal structure developed. *Geophys. J. R. Astron. Soc.,* 39(1):169–187. **doi:10.1111/j.1365-246X.1974.tb05446.x**

Cannat, M., Karson, J.A., Miller, D.J., et al., 1995. *Proc. ODP, Init. Repts.,* 153: College Station, TX (Ocean Drilling Program). **doi:10.2973/odp.proc.ir.153.1995**

Chen, Y.J., 2001. Thermal effects of gabbro accretion from a deeper second melt lens at the fast spreading East Pacific Rise. *J. Geophys. Res., [Solid Earth],* 106(B5):8581–8588. **doi:10.1029/2000JB900420**

Cherkaoui, A.S.M., Wilcock, W.S.D., Dunn, R.A., and Toomey, D.R., 2003. A numerical model of hydrothermal cooling and crustal accretion at a fast spreading mid-ocean ridge. *Geochem., Geophys., Geosyst.,* 4(9):8616. **doi:10.1029/2001GC000215**

Coogan, L.A., in press. The lower oceanic crust. *In* Rudnick, R.L. (Ed.), *Treatise on Geochemistry: The Crust* (Vol. 3). Holland, H.D., and Turekian, K.K. (Series Eds.): New York (Elsevier), 1–45.

Coogan, L.A., 2007. The lower oceanic crust. *In* Rudnick, R.L. (Ed.), *Treatise on Geochemistry: The Crust* (Vol. 3). Holland, H.D., and Turekian, K.K. (Series Eds.): New York (Elsevier), 1–45. **doi:10.1016/B978-008043751-4/00230-3**

Coogan, L.A., Gillis, K.M., MacLeod, C.J., Thompson, G.M., and Hékinian, R., 2002a. Petrology and geochemistry of the lower ocean crust formed at the East Pacific Rise and exposed at Hess Deep: a synthesis and new results. *Geochem., Geophys., Geosyst.,* 3(11):8604. **doi:10.1029/2001GC000230**

Coogan, L.A., and Hinton, R.W., 2006. Do the trace element compositions of detrital zircons require Hadean continental crust? *Geology,* 34(8):633–636. **doi:10.1130/G22737.1**

Coogan, L.A., Jenkin, G.R.T., and Wilson, R.N., 2007a. Contrasting cooling rates in the lower oceanic crust at fast- and slow-spreading ridges revealed by geospeedometry. *J. Petrol.,* 48(11):2211–2231. **doi:10.1093/petrology/egm057**

Coogan, L.A., Kasemann, S.A., and Chakraborty, S., 2005. Rates of hydrothermal cooling of new oceanic upper crust derived from lithium geospeedometry. *Earth Planet. Sci. Lett.,* 240(2):415–424. **doi:10.1016/j.epsl.2005.09.020**

Coogan, L.A., Manning, C.E., and Wilson., R.N., 2007b. Oxygen isotope evidence for short-lived high-temperature fluid flow in the lower oceanic crust at fast-spreading ridges. *Earth Planet. Sci. Lett.,* 260(3–4):524–536. **doi:10.1016/j.epsl.2007.06.013**

Coogan, L.A., Thompson, G., and MacLeod, C.J., 2002b. A textural and geochemical investigation of high level gabbros from the Oman ophiolite: implications for the role of the

axial magma chamber at fast-spreading ridges. *Lithos,* 63(1–2):67–82. **doi:10.1016/S0024-4937(02)00114-7**

Crawford, W.C., and Webb, S.C., 2002. Variations in the distribution of magma in the lower crust and at the Moho beneath the East Pacific Rise at 9°–10°N. *Earth Planet. Sci. Lett.,* 203(1):117–130. **doi:10.1016/S0012-821X(02)00831-2**

Detrick, R.S., Buhl, P., Vera, E., Mutter, J., Orcutt, J., Madsen, J., and Brocher, T., 1987. Multi-channel seismic imaging of a crustal magma chamber along the East Pacific Rise. *Nature (London, U. K.),* 326(6108):35–41. **doi:10.1038/326035a0**

Dick, H.J.B., and Natland, J.H., 1996. Late-stage melt evolution and transport in the shallow mantle beneath the East Pacific Rise. *In* Mével, C., Gillis, K.M., Allan, J.F., and Meyer, P.S. (Eds.), *Proc. ODP, Sci. Results,* 147: College Station, TX (Ocean Drilling Program), 103–134. **doi:10.2973/odp.proc.sr.147.007.1996**

Dick, H.J.B., Natland, J.H., Miller, D.J., et al., 1999. *Proc. ODP, Init. Repts.,* 176: College Station, TX (Ocean Drilling Program). **doi:10.2973/odp.proc.ir.176.1999**

Dunn, R.A., Toomey, D.R., and Solomon, S.C., 2000. Three-dimensional seismic structure and physical properties of the crust and shallow mantle beneath the East Pacific Rise at 9°30′N. *J. Geophys. Res., [Solid Earth],* 105(B10):23537–23556. **doi:10.1029/2000JB900210**

Durant, D.T., and Toomey, D.R., 2009. Evidence and implications of crustal magmatism on the flanks of the East Pacific Rise. *Earth Planet. Sci. Lett.,* 287(1–2):130–136. **doi:10.1016/j.epsl.2009.08.003**

Faak, K., Chakraborty, S., and Coogan, L.A., 2011. Evaluation of the variation in cooling rate with depth in the lower crust at fast-spreading ridges using a newly developed Mg in plagioclase geospeedometer [presented at the 2011 American Geophysical Union Fall Meeting, San Francisco, CA, 5–9 December 2011]. (Abstract V13F-04) **http://www.agu.org/meetings/fm11/waisfm11.html**

Floyd, J.S., Tolstoy, M., Mutter, J.C., and Scholz, C.H., 2002. Seismotectonics of mid-ocean ridge propagation in Hess Deep. *Science,* 298(5599):1765–1768. **doi:10.1126/science.1077950**

Francheteau, J., Armijo, R., Cheminée, J.L., Hekinian, R., Lonsdale, P., and Blum, N., 1990. 1 Ma East Pacific Rise oceanic crust and uppermost mantle exposed by rifting in Hess Deep (equatorial Pacific Ocean). *Earth Planet. Sci. Lett.,* 101(2–4):281–295. **doi:10.1016/0012-821X(90)90160-Y**

Francheteau, J., Armijo, R., Cheminée, J.L., Hekinian, R., Lonsdale, P., and Blum, N., 1992. Dyke complex of the East Pacific Rise exposed in the walls of Hess Deep and the structure of the upper oceanic crust. *Earth Planet. Sci. Lett.,* 111(1):109–121. **doi:10.1016/0012-821X(92)90173-S**

Früh-Green, G.L., Plas, A., and Dell'Angelo, L.N., 1996. Mineralogic and stable isotope record of polyphase alteration of upper crustal gabbros of the East Pacific Rise (Hess Deep, Site 894). *In* Mével, C., Gillis, K.M., Allan, J.F., and Meyer, P.S. (Eds.), *Proc. ODP, Sci. Results,* 147: College Station, TX (Ocean Drilling Program), 235–254. **doi:10.2973/odp.proc.sr.147.015.1996**

Gao, Y., Hoefs, J., Przybilla, R., and Snow, J.E., 2006. A complete oxygen isotope profile through the lower oceanic crust, ODP Hole 735B. *Chem. Geol.,* 233(3–4):217–234. **doi:10.1016/j.chemgeo.2006.03.005**

Garmany, J., 1989. Accumulations of melt at the base of young oceanic crust. *Nature (London, U. K.),* 340(6235):628–632. **doi:10.1038/340628a0**

Gillis, K.M., 1995. Controls on hydrothermal alteration in a section of fast-spreading oceanic crust. *Earth Planet. Sci. Lett.,* 134(3–4):473–489. **doi:10.1016/0012-821X(95)00137-2**

Gillis, K.M., 2008. The roof of an axial magma chamber: a hornfelsic heat exchanger. *Geology,* 36(4):299–302. **doi:10.1130/G24590A.1**

Gillis, K.M., Coogan, L.A., and Chaussidon, M., 2003. Volatile element (B, Cl, F) behaviour in the roof of an axial magma chamber from the East Pacific Rise. *Earth Planet. Sci. Lett.,* 213(3–4):447–462. **doi:10.1016/S0012-821X(03)00346-7**

Gillis, K.M., Coogan, L.A., and Pedersen, R., 2005. Strontium isotope constraints on fluid flow in the upper oceanic crust at the East Pacific Rise. *Earth Planet. Sci. Lett.,* 232(1–2):83–94. **doi:10.1016/j.epsl.2005.01.008**

Gillis, K., Mével, C., Allan, J., et al., 1993. *Proc. ODP, Init. Repts.,* 147: College Station, TX (Ocean Drilling Program). **doi:10.2973/odp.proc.ir.147.1993**

Gillis, K.M., Muehlenbachs, K., Stewart, M., Gleeson, T., and Karson, J., 2001. Fluid flow patterns in fast spreading East Pacific Rise crust exposed at Hess Deep. *J. Geophys. Res., [Solid Earth],* 106(B11):26311–26329. **doi:10.1029/2000JB000038**

Gregory, R.T., and Taylor, H.P., Jr., 1981. An oxygen isotope profile in a section of Cretaceous oceanic crust, Samail ophiolite, Oman: evidence for $\delta^{18}O$ buffering of the oceans by deep (>5 km) seawater-hydrothermal circulation at mid-ocean ridges. *J. Geophys. Res., [Solid Earth],* 86(B4):2737–2755. **doi:10.1029/JB086iB04p02737**

Hanna, H.D., 2004. Geochemical variations in basaltic glasses from an incipient rift and upper level gabbros from Hess Deep, eastern equatorial Pacific [M.Sc. thesis]. Duke Univ., Durham.

Heft, K.L., Gillis, K.M., Pollock, M.A., Karson, J.A., and Klein, E.M., 2008. Role of upwelling hydrothermal fluids in the development of alteration patterns at fast-spreading ridges: evidence from the sheeted dike complex at Pito Deep. *Geochem., Geophys., Geosyst.,* 9(5):Q05O07. **doi:10.1029/2007GC001926**

Hékinian, R., Bideau, D., Francheteau, J., Cheminee, J.L., Armijo, R., Lonsdale, P., and Blum, N., 1993. Petrology of the East Pacific Rise crust and upper mantle exposed in Hess Deep (eastern equatorial Pacific). *J. Geophys. Res., [Solid Earth],* 98(B5):8069–8094. **doi:10.1029/92JB02072**

Henstock, T.J., Woods, A.W., and White, R.S., 1993. The accretion of oceanic crust by episodic sill intrusion. *J. Geophys. Res., [Solid Earth],* 98(B3):4143–4161. **doi:10.1029/92JB02661**

Hess, H.H., 1960. The AMSOC hole to the Earth's mantle. *Am. Sci.,* 48(2):254–263. **http://www.jstor.org/stable/27827541**

Hey, R., Johnson, G.L., and Lowrie, A., 1977. Recent plate motions in the Galapagos area. *Geol. Soc. Am. Bull.,* 88(10):1385–1403. **doi:10.1130/0016-7606(1977)88<1385:RPMITG>2.0.CO;2**

Hey, R.N., Deffeyes, K.S., Johnson, G.L., and Lowrie, A., 1972. The Galapagos triple junction and plate motions in the East Pacific. *Nature (London, U. K.),* 237(5349)20–22. **doi:10.1038/237020a0**

Holden, J.C., and Dietz, R.S., 1972. Galapagos gore, NazCoPac triple junction and Carnegie/Cocos Ridges. *Nature (London, U. K.),* 235(5336):266–269. **doi:10.1038/235266a0**

Hooft, E.E.E., Detrick, R.S., and Kent, G.M., 1994. Seismic structure and indicators of magma budget along the southern East Pacific Rise. *J. Geophys. Res., [Solid Earth],* 102(B12):27319–27340. **doi:10.1029/97JB02349**

John, B.E., Foster, D.A., Murphy, J.M., Cheadle, M.J., Baines, A.G., Fanning, C.M., and Copeland, P., 2004. Determining the cooling history of in situ lower oceanic crust—Atlantis

Bank, SW Indian Ridge. *Earth Planet. Sci. Lett.,* 222(1):145–160. **doi:10.1016/j.epsl.2004.02.014**

Karson, J.A., Hurst, S.D., and Lonsdale, P., 1992. Tectonic rotations of dikes in fast-spread oceanic crust exposed near Hess Deep. *Geology,* 20(8):685–688. **doi:10.1130/0091-7613(1992)020<0685:TRODIF>2.3.CO;2**

Karson, J.A., Klein, E.M., Hurst, S.D., Lee, C.E., Rivizzigno, P.A., Curewitz, D., Morris, A.R., Miller, D.J., Varga, R.G., Christeson, G.L., Cushman, B., O'Neill, J.M., Brophy, J.G., Gillis, K.M., Stewart, M.A., and Sutton, A.L., 2002. Structure of uppermost fast-spread oceanic crust exposed at the Hess Deep Rift: implications for subaxial processes at the East Pacific Rise. *Geochem., Geophys., Geosyst.,* 3(1):1002. **doi:10.1029/2001GC000155**

Kelemen, P.B., and Aharonov, E., 1998. Periodic formation of magma fractures and generation of layered gabbros in the lower crust beneath oceanic spreading centers. *In* Buck, R., Delaney, P.T., Karson, J.A., and Lagabrielle, Y. (Eds.), *Faulting and Magmatism at Mid-Ocean Ridges*. Geophys. Monogr., 106:267–289. **doi:10.1029/GM106p0267**

Kelemen, P.B., Kikawa, E., Miller, D.J., et al., 2004. *Proc. ODP, Init. Repts.,* 209: College Station, TX (Ocean Drilling Program). **doi.10.2973/odp.proc.ir.209.2004**

Kelemen, P.B., Koga, K., and Shimizu, N., 1997. Geochemistry of gabbro sills in the crust-mantle transition zone of the Oman ophiolite: implications for the origin of the oceanic lower crust. *Earth Planet. Sci. Lett.,* 146(3–4):475–488. **doi:10.1016/S0012-821X(96)00235-X**

Kelley, D.S., and Malpas, J., 1996. Melt-fluid evolution in gabbroic rocks from Hess Deep. *In* Mével, C., Gillis, K.M., Allan, J.F., and Meyer, P.S. (Eds.), *Proc. ODP, Sci. Results,* 147: College Station, TX (Ocean Drilling Program), 213–226. **doi:10.2973/odp.proc.sr.147.013.1996**

Kent, G.M., Harding, A.J., and Orcutt, J.A., 1990. Evidence for a smaller magma chamber beneath the East Pacific Rise at 9°30′N. *Nature (London, U. K.),* 344(6267):650–653. **doi:10.1038/344650a0**

Kirchner, T., and Gillis, K.M., in press. Mineralogical and strontium isotopic record of hydrothermal processes in the lower ocean crust at and near the East Pacific Rise. *Contrib. Mineral. Petrol.*

Klein, E.M., 2007. Geochemistry of the igneous ocean crust. *In* Rudnick, R.L. (Ed.), *Treatise on Geochemistry*: *The Crust* (Vol. 3). Holland, H.D., and Turekian, K.K. (Series Eds.): New York (Elsevier), 433–463. **doi:10.1016/B0-08-043751-6/03030-9**

Koepke, J., Berndt, J., Feig, S.T., and Holtz, F., 2007. The formation of SiO_2-rich melts within the deep ocean crust by hydrous partial melting of gabbros. *Contrib. Mineral. Petrol.,* 153(1):67–84. **doi:10.1007/s00410-006-0135-y**

Koepke, J., France, L., Müller, T., Faure, F., Goetze, N., Dziony, W., and Ildefonse, B., 2011. Gabbros from IODP Site 1256, equatorial Pacific: insight into axial magma chamber processes at fast-spreading ocean ridges. *Geochem., Geophys., Geosyst.,* 12(9):Q09014. **doi:10.1029/2011GC003655**

Korenaga, J., and Kelemen, P.B., 1997. Origin of gabbro sills in the Moho transition zone of the Oman ophiolite: implications for magma transport in the oceanic lower crust. *J. Geophys. Res., [Solid Earth],* 102(B12):27729–27749. **doi:10.1029/97JB02604 doi:10.1029/97JB02604**

Korenaga, J., and Kelemen, P.B., 1998. Melt migration through the oceanic lower crust: a constraint from melt percolation modeling with finite solid diffusion. *Earth Planet. Sci. Lett.,* 156(1–2):1–11. **doi:10.1016/S0012-821X(98)00004-1**

Lécuyer, C., and Gruau, G., 1996. Oxygen and strontium isotope compositions of Hess Deep gabbros (Holes 894F and 894G): high-temperature interaction of seawater with the oceanic crust Layer 3. *In* Mével, C., Gillis, K.M., Allan, J.F., and Meyer, P.S. (Eds.), *Proc. ODP, Sci. Results,* 147: College Station, TX (Ocean Drilling Program), 227–234. **doi:10.2973/odp.proc.sr.147.014.1996**

Lecuyer, C., and Reynard, B., 1996. High-temperature alteration of oceanic gabbros by seawater (Hess Deep, Ocean Drilling Program Leg 147): evidence from oxygen isotopes and elemental fluxes. *J. Geophys. Res., [Solid Earth],* 101(B7):15883–15897. **doi:10.1029/96JB00950**

Lonsdale, P., 1988. Structural pattern of the Galapagos microplate and evolution of the Galapagos triple junctions. *J. Geophys. Res. [Solid Earth],* 93(B11):13551–13574. **doi:10.1029/JB093iB11p13551**

Lonsdale, P., 1989. Segmentation of the Pacific-Nazca spreading center, 1°N–20°S. *J. Geophys. Res., [Solid Earth],* 94(B9):12197–12225. **doi:10.1029/JB094iB09p12197**

Maclennan, J., Hulme, T., and Singh, S.C., 2004. Thermal models of oceanic crustal accretion: linking geophysical, geological, and petrological observations. *Geochem., Geophys., Geosyst.,* 5(2):Q02F25. **doi:10.1029/2003GC000605**

MacLeod, C.J., Boudier, F., Yaouancq, G., and Richter, C., 1996a. Gabbro fabrics from Site 894, Hess Deep: implications for magma chamber processes at the East Pacific Rise. *In* Mével, C., Gillis, K.M., Allan, J.F., and Meyer, P.S. (Eds.), *Proc. ODP, Sci. Results,* 147: College Station, TX (Ocean Drilling Program), 317–328. **doi:10.2973/odp.proc.sr.147.018.1996**

MacLeod, C.J., Célérier, B., Früh-Green, G.L., and Manning, C.E., 1996b. Tectonics of Hess Deep: a synthesis of drilling results from Leg 147. *In* Mével, C., Gillis, K.M., Allan, J.F., and Meyer, P.S. (Eds.), *Proc. ODP, Sci. Results,* 147: College Station, TX (Ocean Drilling Program), 461–475. **doi:10.2973/odp.proc.sr.147.032.1996**

MacLeod, C.J., Teagle, D.A., Gillis, K.M., Shillington, D.J., and Scientific Party, 2008. Morphotectonics of Hess Deep: preliminary results of RSS *James Cook* Cruise JC21. *Eos, Trans. Am. Geophys. Union,* 89(53)(Suppl.):V43I-408. (Abstract) **http://www.agu.org/meetings/fm08/waisfm08.html**

MacLeod, C.J., and Yaouancq, G., 2000. A fossil melt lens in the Oman ophiolite: implications for magma chamber processes at fast spreading ridges. *Earth Planet. Sci. Lett.,* 176(3–4):357–373. **doi:10.1016/S0012-821X(00)00020-0**

Manning, C.E., and MacLeod, C.J., 1996. Fracture-controlled metamorphism of Hess Deep gabbros, Site 894: constraints on the roots of mid-ocean-ridge hydrothermal systems at fast-spreading centers. *In* Mével, C., Gillis, K.M., Allan, J.F., and Meyer, P.S. (Eds.), *Proc. ODP, Sci. Results,* 147: College Station, TX (Ocean Drilling Program), 189–212. **doi:10.2973/odp.proc.sr.147.011.1996**

Manning, C.E., Weston, P.E., and Mahon, K.I., 1996. Rapid high-temperature metamorphism of East Pacific Rise gabbros from Hess Deep. *Earth Planet. Sci. Lett.,* 144(1–2):123–132. **doi:10.1016/0012-821X(96)00153-7**

McCollom, T.M., and Shock, E.L., 1998. Fluid-rock interactions in the lower oceanic crust: thermodynamic models of hydrothermal alteration. *J. Geophys. Res., [Solid Earth],* 103(B1):547–576. **doi:10.1029/97JB02603**

Mitchell, G.A., Montési, L.G.J., Zhu, W., Smith, D.K., and Schouten, H., 2011. Transient rifting north of the Galápagos triple junction. *Earth. Planet. Sci. Lett.,* 307(3–4):461–469. **doi:10.1016/j.epsl.2011.05.027**

Morton, J.L., and Sleep, N.H., 1985. A mid-ocean ridge thermal model: constraints on the volume of axial hydrothermal heat flux. *J. Geophys. Res., [Solid Earth],* 90(B13):11345–11353. **doi:10.1029/JB090iB13p11345**

Natland, J.H., and Dick, H.J.B., 1996. Melt migration through high-level gabbroic cumulates of the East Pacific Rise at Hess Deep: the origin of magma lenses and the deep crustal structure of fast-spreading ridges. *In* Mével, C., Gillis, K.M., Allan, J.F., and Meyer, P.S. (Eds.), *Proc. ODP, Sci. Results,* 147: College Station, TX (Ocean Drilling Program), 21–58. **doi:10.2973/odp.proc.sr.147.002.1996**

Nicolas, A., 1989. *Structures of Ophiolites and Dynamics of Oceanic Lithosphere*: Dordrecht (Springer).

Nicolas, A., Reuber, I., and Benn, K., 1988. A new magma chamber model based on structural studies in the Oman ophiolite. *Tectonophysics,* 151(1–4):87–105. **doi:10.1016/0040-1951(88)90242-9**

Ocean Drilling Program, 1995. Report of the Offset Drilling Workshop. *ODP Tech. Note,* 25. **doi:10.2973/odp.tn.25.1995**

O'Hara, M.J., 1968. Are ocean floor basalts primary magma? *Nature (London, U. K.),* 220(5168):683–686. **doi:10.1038/220683a0**

Pallister, J.S., and Hopson, C.A., 1981. Samail ophiolite plutonic suite: field relations, phase variation, cryptic variation and layering, and a model of a spreading ridge magma chamber. *J. Geophys. Res., [Solid Earth],* 86(B4):2593–2644. **doi:10.1029/JB086iB04p02593**

Pariso, J.E., Kelso, P., and Richter, C., 1996. Paleomagnetism and rock magnetic properties of gabbro from Hole 894G, Hess Deep. *In* Mével, C., Gillis, K.M., Allan, J.F., and Meyer, P.S. (Eds.), *Proc. ODP, Sci. Results,* 147: College Station, TX (Ocean Drilling Program), 373–381. **doi:10.2973/odp.proc.sr.147.023.1996**

Pedersen, R.B., Malpas, J., and Falloon, T., 1996. Petrology and geochemistry of gabbroic and related rocks from Site 894, Hess Deep. *In* Mével, C., Gillis, K.M., Allan, J.F., and Meyer, P.S. (Eds.), *Proc. ODP, Sci. Results,* 147: College Station, TX (Ocean Drilling Program), 3–19. **doi:10.2973/odp.proc.sr.147.001.1996**

Perk, N.W., Coogan, L.A., Karson, J.A., Klein, E.M., and Hanna, H.D., 2007. Petrology and geochemistry of primitive lower oceanic crust from Pito Deep: implications for the accretion of the lower crust at the southern East Pacific Rise. *Contrib. Mineral. Petrol.,* 154(5):575–590. **doi:10.1007/s00410-007-0210-z**

Phipps Morgan, J., and Chen, Y.J., 1993. The genesis of oceanic crust: magma injection, hydrothermal circulation, and crustal flow. *J. Geophys. Res., [Solid Earth],* 98(B4):6283–6297. **doi:10.1029/92JB02650**

Quick, J.E., and Denlinger, R.P., 1993. Ductile deformation and the origin of layered gabbro in ophiolites. *J. Geophys. Res., [Solid Earth],* 98(B8):14015–14027. **doi:10.1029/93JB00698**

Richter, C., Kelso, P.R., and MacLeod, C.J., 1996. Magnetic fabrics and sources of magnetic susceptibility in lower crustal and upper mantle rocks from Hess Deep. *In* Mével, C., Gillis, K.M., Allan, J.F., and Meyer, P.S. (Eds.), *Proc. ODP, Sci. Results,* 147: College Station, TX (Ocean Drilling Program), 393–403. **doi:10.2973/odp.proc.sr.147.025.1996**

Robinson, P.T., Von Herzen, R., et al., 1989. *Proc. ODP, Init. Repts.,* 118: College Station, TX (Ocean Drilling Program). **doi:10.2973/odp.proc.ir.118.1989**

Ryan, W.B.F., Carbotte, S.M., Coplan, J.O., O'Hara, S., Melkonian, A., Arko, R., Weissel, R.A., Ferrini, V., Goodwillie, A., Nitsche, F., Bonczkowski, J., and Zemsky, R., 2009. Global multi-resolution topography synthesis. *Geochem., Geophys., Geosyst.,* 10(3):Q03014. **doi:10.1029/2008GC002332**

Schouten, H., Smith, D.K., Montési, L.G.J., Zhu, W., and Klein, E.M., 2008. Cracking of lithosphere north of the Galapagos triple junction. *Geology,* 36(5):339–342. **doi:10.1130/G24431A.1**

Singh, S.C., Kent, G.M., Collier, J.S., Harding, A.J., and Orcutt, J.A., 1998. Melt to mush variations in crustal magma properties along the ridge crest at the southern East Pacific Rise. *Nature (London, U. K.),* 394(6696):874–878. **doi:10.1038/29740**

Sleep, N.H., 1975. Formation of oceanic crust: some thermal constraints. *J. Geophys. Res., [Solid Earth],* 80(29):4037–4042. **doi:10.1029/JB080i029p04037**

Smith, D.K., Schouten, H., Zhu, W., Montési, L.G.J., and Cann, J.R., 2011. Distributed deformation ahead of the Cocos-Nazca Rift at the Galapagos triple junction. *Geochem., Geophys., Geosyst.,* 12(6):Q11003. **doi:10.1029/2011GC003689**

Stewart, M.A., Karson, J.A., and Klein, E.M., 2005. Four-dimensional upper crustal construction at fast-spreading mid-ocean ridges: a perspective from an upper crustal cross-section at the Hess Deep Rift. *J. Volcanol. Geotherm. Res.,* 144(1–4):287–309. **doi:10.1016/j.jvolgeores.2004.11.026**

Stewart, M.A., Klein, E.M., and Karson, J.A., 2002. Geochemistry of dikes and lavas from the north wall of the Hess Deep Rift: insights into the four-dimensional character of crustal construction at fast-spreading mid-ocean ridges. *J. Geophys. Res., [Solid Earth],* 107(B10):2238. **doi:10.1029/2001JB000545**

Stolper, E., and Walker, D., 1980. Melt density and the average composition of basalt. *Contrib. Mineral. Petrol.,* 74(1):7–12. **doi:10.1007/BF00375484**

Teagle, D.A.H., Alt, J.C., and Halliday, A.N., 1998. Tracing the chemical evolution of fluids during hydrothermal recharge: constraints from anhydrite recovered in ODP Hole 504B. *Earth Planet. Sci. Lett.,* 155(3–4):167–182. **doi:10.1016/S0012-821X(97)00209-4**

Teagle, D.A.H., Bickle, M.J., and Alt, J.C., 2003. Recharge flux to ocean-ridge black smoker systems: a geochemical estimate from ODP Hole 504B. *Earth Planet. Sci. Lett.,* 210(1–2):81–89. **doi:10.1016/S0012-821X(03)00126-2**

Wager, L.R., and Brown, G.M., 1967. *Layered Igneous Rocks:* San Francisco (W.H. Freeman).

Wager, L.R., Brown, G.M., and Wadsworth, W.J., 1960. Types of igneous cumulates. *J. Petrol.,* 1(1):73–85. **http://petrology.oxfordjournals.org/content/1/1/73.abstract**

Wiggins, S.M., Dorman, L.M., Cornuelle, B.D., and Hildebrand, J.A., 1996. Hess Deep rift valley structure from seismic tomography. *J. Geophys. Res., [Solid Earth],* 101(B10):22335–22353. **doi:10.1029/96JB01230**

Wilson, D.S., Teagle, D.A.H., Alt, J.C., Banerjee, N.R., Umino, S., Miyashita, S., Acton, G.D., Anma, R., Barr, S.R., Belghoul, A., Carlut, J., Christie, D.M., Coggon, R.M., Cooper, K.M., Cordier, C., Crispini, L., Durand, S.R., Einaudi, F., Galli, L., Gao, Y., Geldmacher, J., Gilbert, L.A., Hayman, N.W., Herrero-Bervera, E., Hirano, N., Holter, S., Ingle, S., Jiang, S., Kalberkamp, U. Kerneklian, M., Koepke, J., Laverne, C., Vasquez, H.L.L., Maclennan, J., Morgan, S., Neo, N., Nichols, H.J., Park, S.-H., Reichow, M.K., Sakuyama, T., Sano, T., Sandwell, R., Scheibner, B., Smith-Duque, C.E., Swift, S.A., Tartarotti, P., Tikku, A.A., Tominaga, M., Veloso, E.A., Yamasaki, T., Yamazaki, S., and Ziegler, C., 2006. Drilling to gabbro in intact ocean crust. *Science,* 312(5776):1016–1020. **doi:10.1126/science.1126090**

Zonenshain, L.P., Kogan, L.I., Savostin, L.A., Golmstock, A.J., and Gorodnitskii, A.M., 1980. Tectonics, crustal structure and evolution of the Galapagos triple junction. *Mar. Geol.,* 37(3–4):209–230. **doi:10.1016/0025-3227(80)90102-4**

Table T1. Model operations plan and time estimate, Expedition 345.

Site	Location Latitude Longitude	Seafloor Depth (mbrf)	Operations Description		Transit (days)	Drilling Coring (days)	Wireline Logging (days)
Puntarenas, Costa Rica			Begin Expedition	5	Port Call Days		
			Transit ~1098 nmi to HD-01A @ 10.5 kt		4.4		
HD-01B	2° 15.175' N	4855	Hole A - Pilot Hole			3.4	0.0
	101° 32.570' W		RCB core 50-100 meters into basement to determine sediment				
			thickness and the basic nature of upper basement hole stability				
			- multiple pilot holes likely required				
			Hole B - Reentry Hole			20.3	1.0
			Deploy reentry cone and short 20 inch conductor casing				
			Reenter and drill 18.5 inch diameter hole 6-10 m (?) into basement				
			Reenter and cement 16 inch casing 5-6 m (?) into basement				
			Reenter, drill out cement, and RCB core to ~340 mbsf (3 bit runs)				
			Conduct downhole wireline logging (two tool strings)				
			Sub-Total Days On-Site:	24.7			
			Note: Primary goal is to establish a hole that can be reentered multiple times, allow formation stability to be maintained, and core that hole as deeply as possible. If this occurs then all remaining available time will be spent on that hole and other holes/sites will not be established.				
			Transit ~0 nmi to HD-02A @ 1.5 kt		0.0		
HD-02B	2° 15.138' N	4860	Hole A - Pilot Hole			3.4	0.0
	101° 32.750' W		RCB core 50-100 meters into basement to determine sediment				
			thickness and the basic nature of upper basement hole stability				
			Hole B - Reentry Hole			16.9	0.9
			Deploy reentry cone and short 20 inch conductor casing				
			Reenter and drill 18.5 inch diameter hole 6-10 m (?) into basement				
			Reenter and cement 16 inch casing 5-6 m (?) into basement				
			Reenter, drill out cement, and RCB core to ~265 mbsf (3 bit runs)				
			Conduct downhole wireline logging (two tool strings)				
			Sub-Total Days On-Site:	21.3			
			Transit ~1343 nmi to waypoint @ 10.5		5.3		
			Transit ~94 nmi to Balboa @ 10.5		0.4		
Balboa, Panama			End Expedition		10.1	44.1	1.9

Port Call:	5.0	Total Operating Days:	56.0		
Sub-Total On-Site:	46.0	Total Expedition:	61.0		

This table is a model only. It is likely that the sequence of operations will be different. See **"Drilling strategy and operations plan"** for explanation. The single primary goal of our expedition is to establish a hole that can be reentered multiple times, allow formation stability to be maintained, and core/log that hole as deeply as possible. When this occurs, all remaining available time may be spent on this hole and other holes/sites will not be established. RCB = rotary core barrel.

Figure F1. Schematic of existing basement holes that have major penetrations into the ocean crust and upper mantle as a function of spreading rate. The lithologic units are schematically distributed vertically, meaning that the total crustal thickness and the depth of lithologic transitions are not constant with spreading rate. The vertical axis therefore is not intended to imply true crustal thickness. The relative lengths of the bars for each site indicate the maximum thickness of penetration for each hole. Dominant rock types are color-coded: green = peridotite, yellow = gabbro, red = basalt.

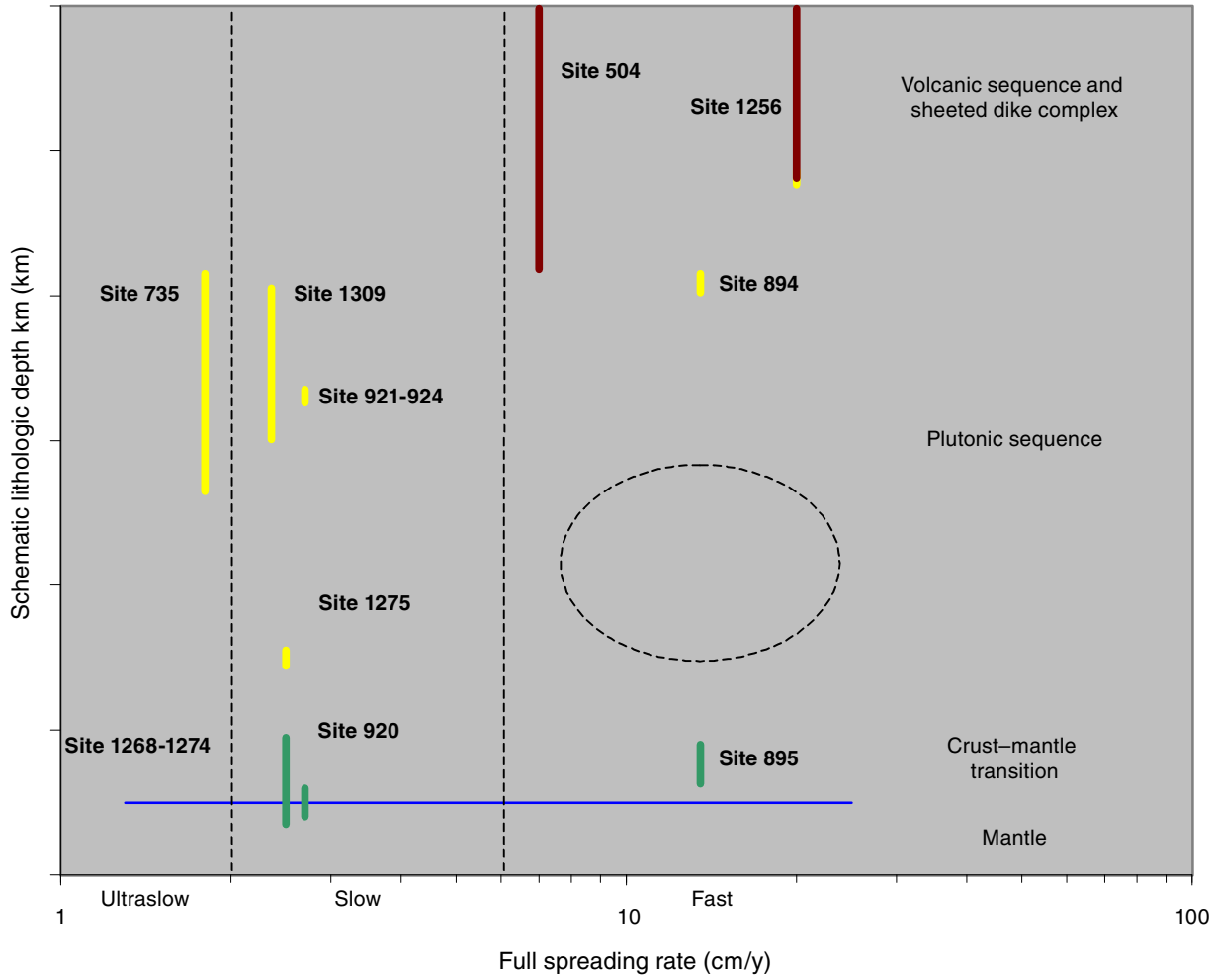

Figure F2. Models for the formation of the lower oceanic crust. Note the dramatically different distribution of hydrothermal heat extraction in the two models caused by the difference in where the latent heat of crystallization of the lower crust is released. Figure modified from Coogan (in press). **A.** A "gabbro-glacier" model (Quick and Denlinger, 1993; Phipps Morgan and Chen, 1993; Henstock et al., 1993) in which the lower oceanic crust crystallizes in a thin magma lens at the base of the sheeted dike complex from which cumulates subside downwards and outwards to form the lower crust. **B.** A "sheeted sill" model (Bédard et al., 1988; Kelemen et al., 1997) in which the lower oceanic crust forms through the crystallization of multiple sills.

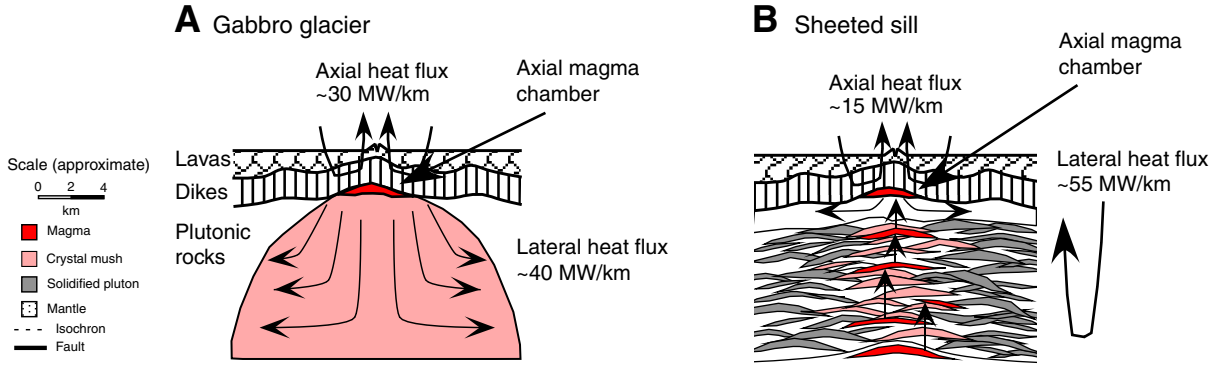

Figure F3. Map of the Galapagos triple junction in the eastern equatorial Pacific showing bathymetry derived from satellite altimetry data and archived multibeam bathymetry data available from the Global MultiResolution Topography Data Portal at Lamont Doherty Earth Observatory. The map was generated using GeoMapApp (Ryan et al., 2009). Tectonic boundaries modified from Smith et al. (2011).Red box with dashed lines indicates location of the map in Figure **F4.** EPR = East Pacific Rise, TJ = triple junction.

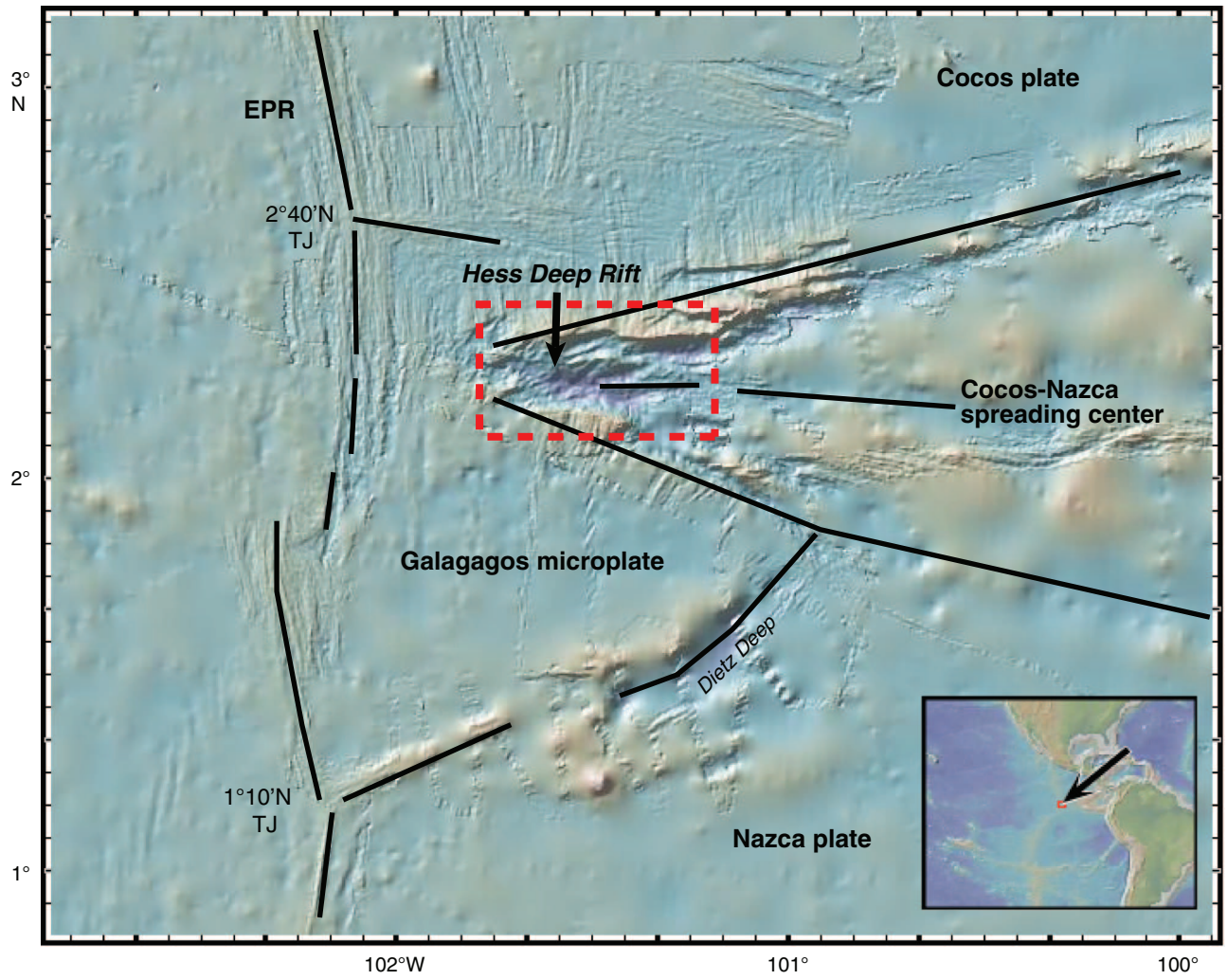

Figure F4. Regional bathymetric map of the Hess Deep Rift showing key morphological features and locations of ODP Sites 894/895 and Expedition 345 proposed Sites HD-01B–HD-04B. Boxes indicate where smaller scale maps of the western end of the intrarift ridge and the southernmost slope of the intrarift ridge are shown in Figures **F5** and **F6.** Regional multibeam bathymetry data were acquired using the hull-mounted Kongsberg Simrad EM120/SBP120 system (12 kHz). Newly acquired swath data were gridded at between 50 and 150 m depending on the density of data coverage, with the smallest grid spacing in the center of Hess Deep, and combined with existing swath data in this region available from the Marine Geoscience Data System (**www.marine-geo.org**). Existing data were from cruises aboard the R/V *Thomas Washington* in 1982 (principle investigator [PI]: P. Lonsdale), 1985 (PI: P. Lonsdale), and 1992 (PI: L. Dorman) and aboard the R/V *Melville* in 2000 (PI: D. Fornari) and 2002 (PI: E. Klein). Map prepared by D. Shillington and V. Ferrini.

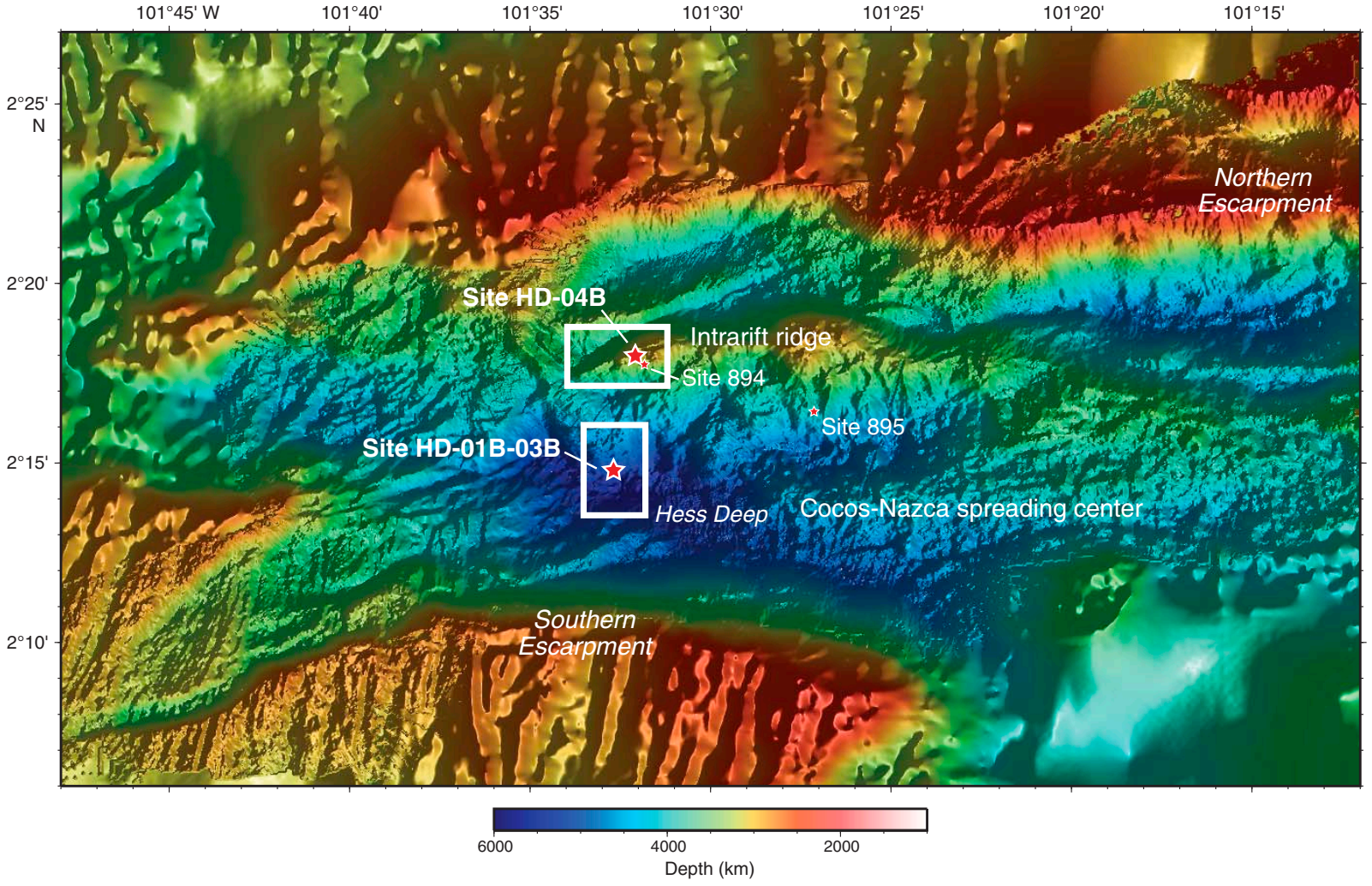

Figure F5. Contoured, microbathymetry map for southern slope between 4300 and 5400 mbsl showing the location of proposed Sites HD-01B–HD-03B and the location and rock type for samples recovered by the ROV *Isis* (MacLeod et al., unpubl. cruise report, 2008). Rock types were determined by shore-based petrographic analysis (C. MacLeod, unpubl. data, 2009). Microbathymetry data were acquired at a nominal altitude of ~100 m and speed of 0.3 kt by a Simrad SM2000 (200 kHz) multibeam sonar system mounted on the *Isis*. Swath widths during *Isis* surveys were ~200–350 m depending on noise and seabed characteristics (dip and reflectivity). See Figure **F4** for location within the Hess Deep Rift. Detailed bathymetry and geology of the sedimented bench in the vicinity of the drill sites outlined by the dashed line is shown in Figure **F8.** Note that the NazCoPac samples are not shown because their locations are not precisely known. Map prepared by D. Shillington and V. Ferrini. (Figure shown on next page.)

Figure F5 (continued). (Caption shown on previous page.)

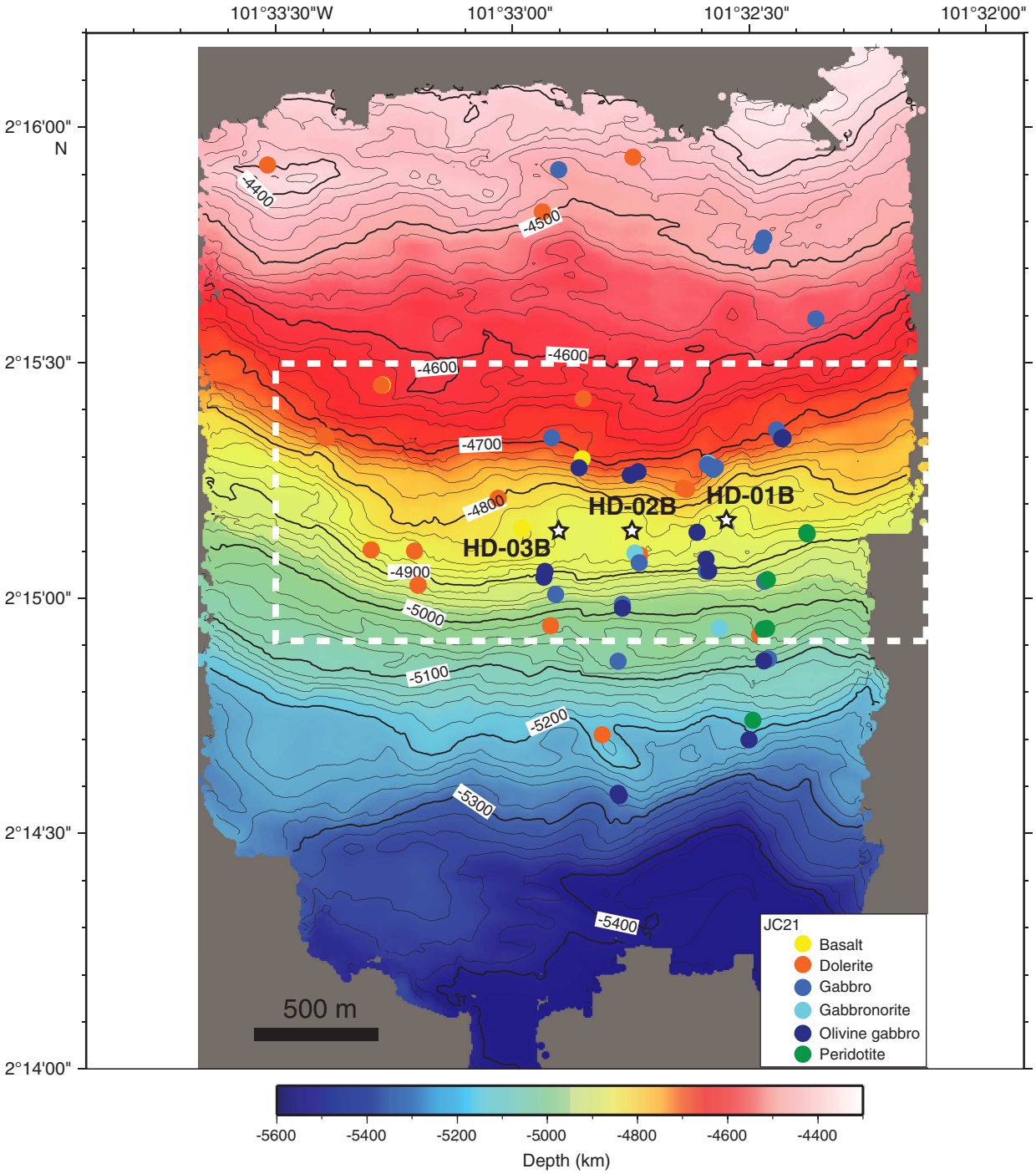

Figure F6. Contoured bathymetry map for the summit of the intrarift ridge showing the location of proposed drill site and the location and rock type for samples recovered by the ROV *Isis*. Rock types were determined by shore-based petrographic analysis (C. MacLeod, unpubl. data, 2009). Contour interval is 20 m. See Figure F4 for location. Map prepared by D. Shillington and V. Ferrini.

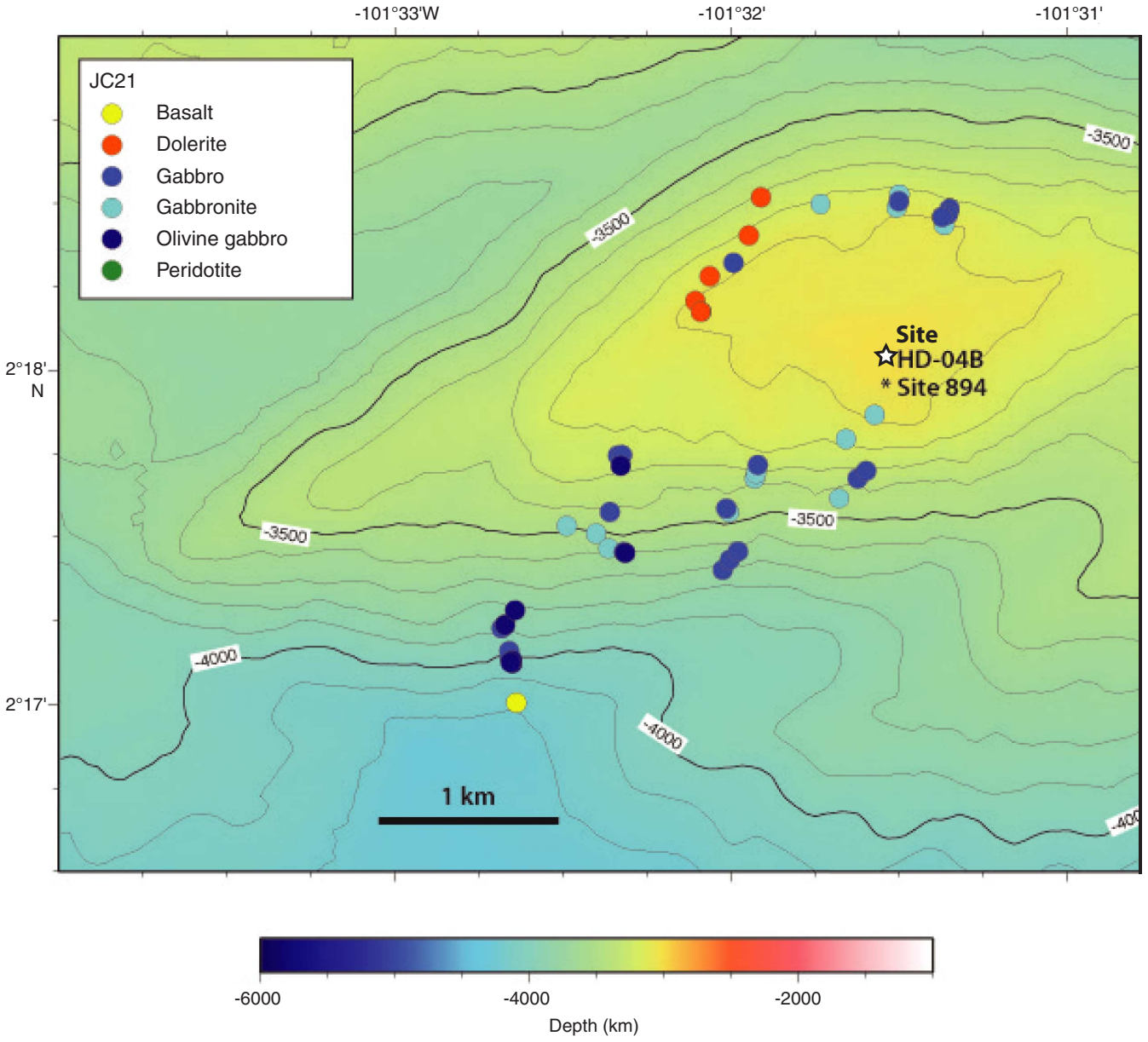

Figure F7. Bulk rock Mg# versus depth for Hess Deep Rift gabbroic rocks. Note that the base of the sheeted dike complex occurs at ~2900 mbsl along the Northern Escarpment and at ~3000 mbsl at the intrarift ridge. Data sources: ODP Site 894 (Pedersen et al., 1996), Cruise JC021 (C. MacLeod, unpubl. data, 2009), NazCoPac cruise (Blum, 1991), Northern Escarpment (Hanna, 2004; Natland and Dick, 1996). IR = intrarift ridge.

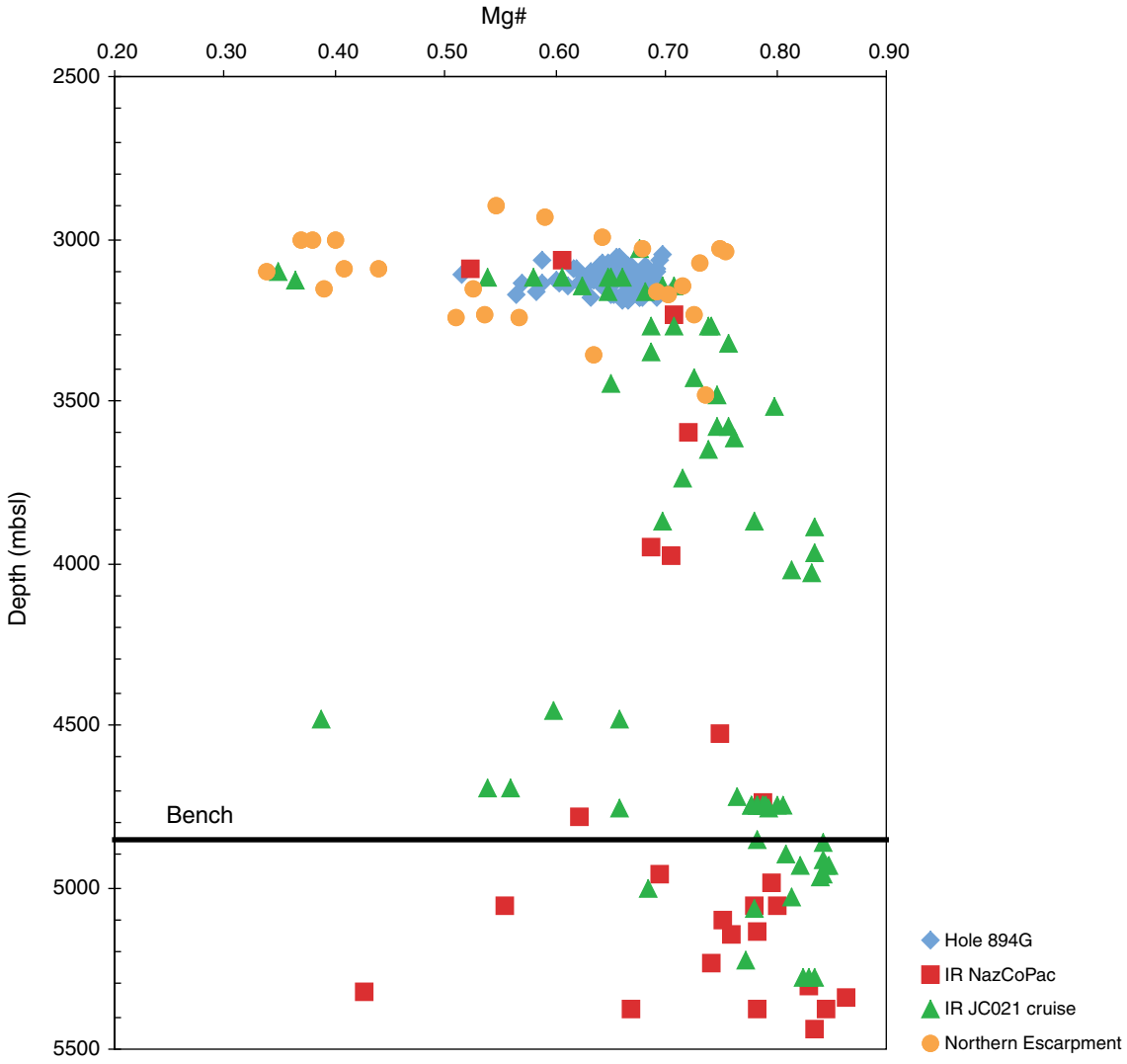

Figure F8. A. Contoured microbathymetry map of the sedimented bench in the vicinity of the drill sites. **B.** Illuminated microbathymetry map of the sedimented bench showing the location of the drill sites and rock types for samples recovered by the ROV *Isis* (MacLeod et al., unpubl. cruise report, 2008). Contour interval = 20 m. **C.** Three north–south seafloor depth profiles centered at each drill site. We assume that the slope above the bench is the footwall of a normal fault that projects beneath the bench. The depth of the normal fault beneath the center of the bench (listed on each panel) is constrained in two ways: (1) the upper slope is projected beneath the bench——this constrains the minimum depth of the fault below the bench, and (2) a slope of 60° (i.e., expected slope of a normal fault prior to erosion) is projected beneath the bench—this constrains the maximum depth of the fault below the bench (120–263 mbsf at proposed Site HD-01B; 87–208 mbsf at proposed Site HD-02B; 97–269 mbsf at proposed Site HD-03B). Map prepared by D. Shillington and V. Ferrini. (Figure shown on next page.)

Figure F8 (continued). (Caption shown on previous page.)

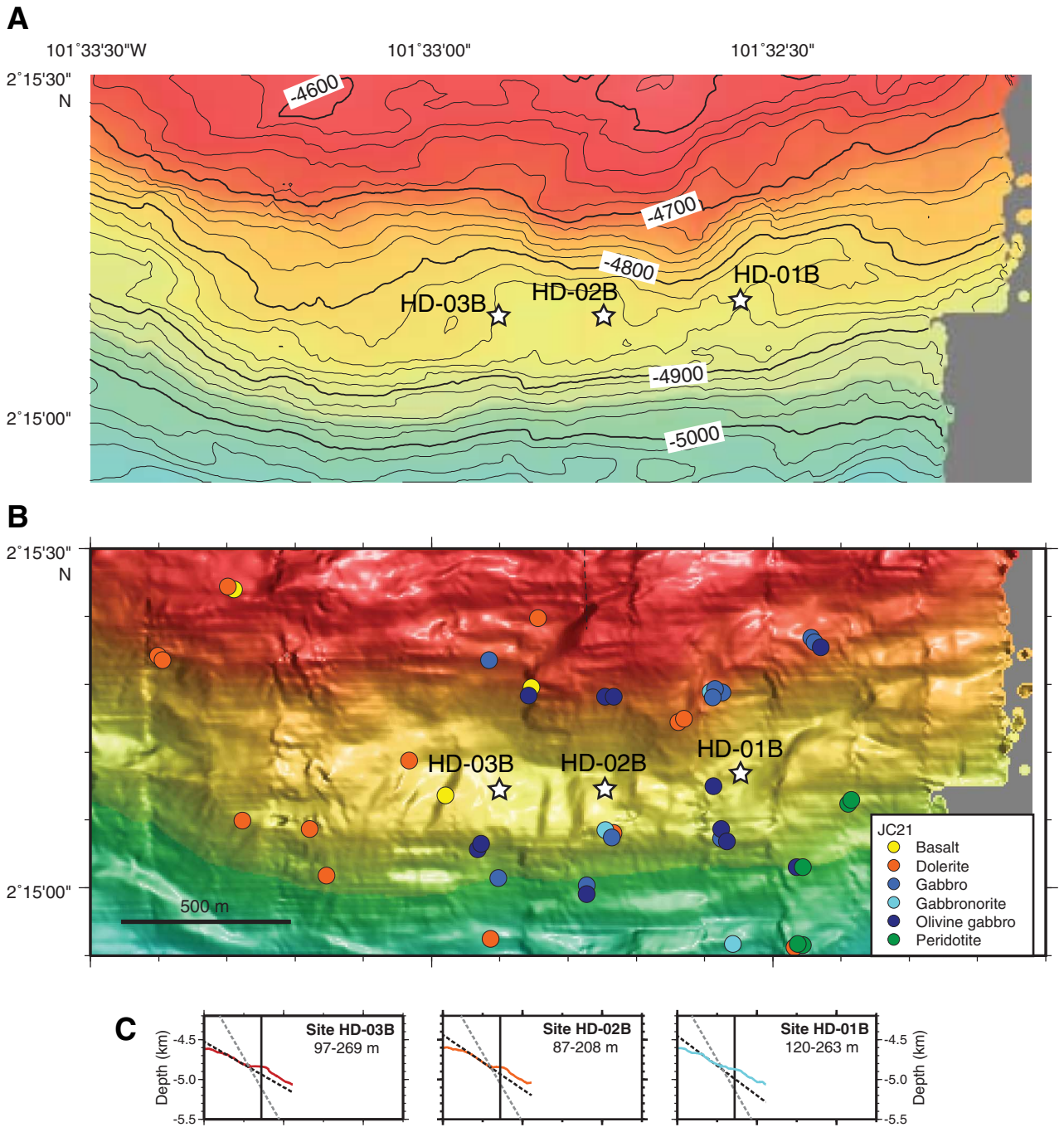

Figure F9. Schematic cartoon of a standard reentry cone and casing used for initiating a borehole that facilitates multiple re-entries and allows additional casing strings to stabilize uppermost basement. See **"Drilling strategy and operations plan"** for explanation of operational approaches to be used to address expected drilling challenges.

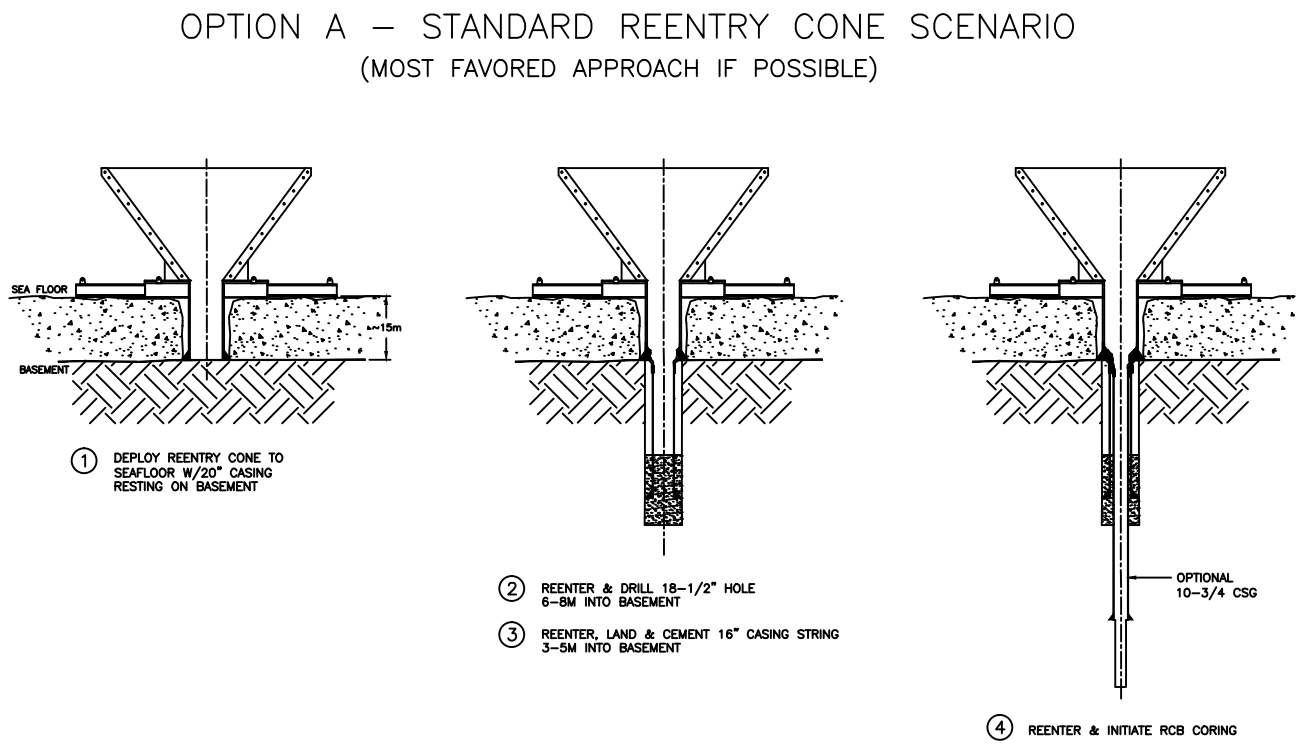

Figure F10. Schematic cartoon of a modified free-fall funnel (FFF) used for initiating a borehole that facilitates multiple re-entries. See **"Drilling strategy and operations plan"** for explanation of operational approaches to be used to address expected drilling challenges.

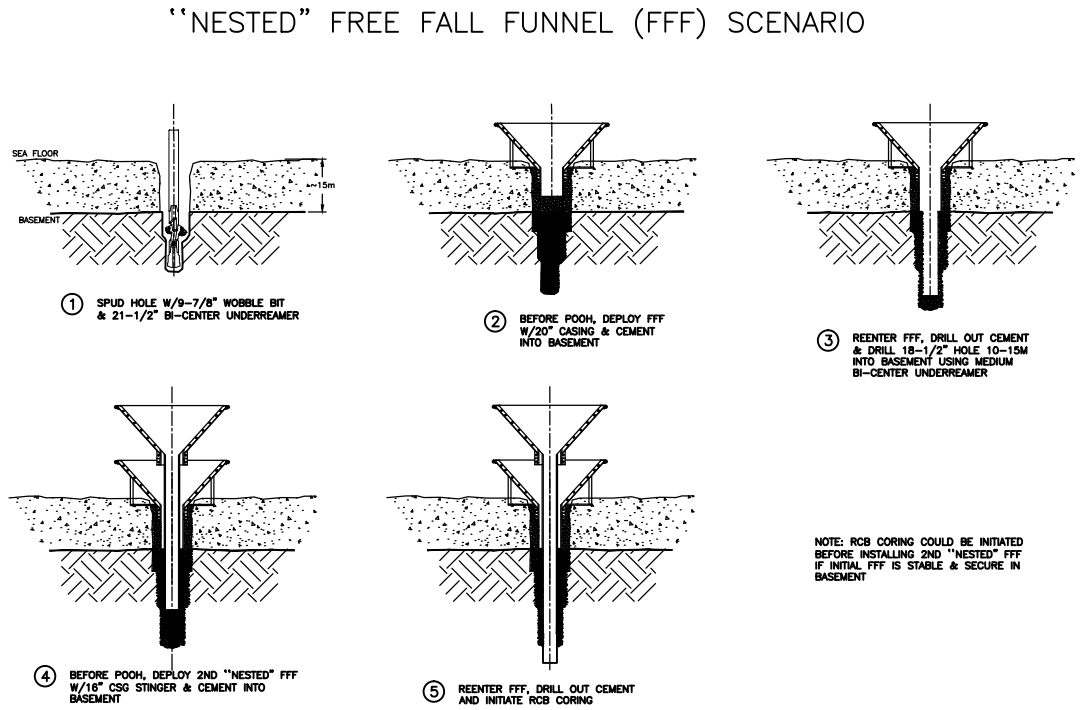

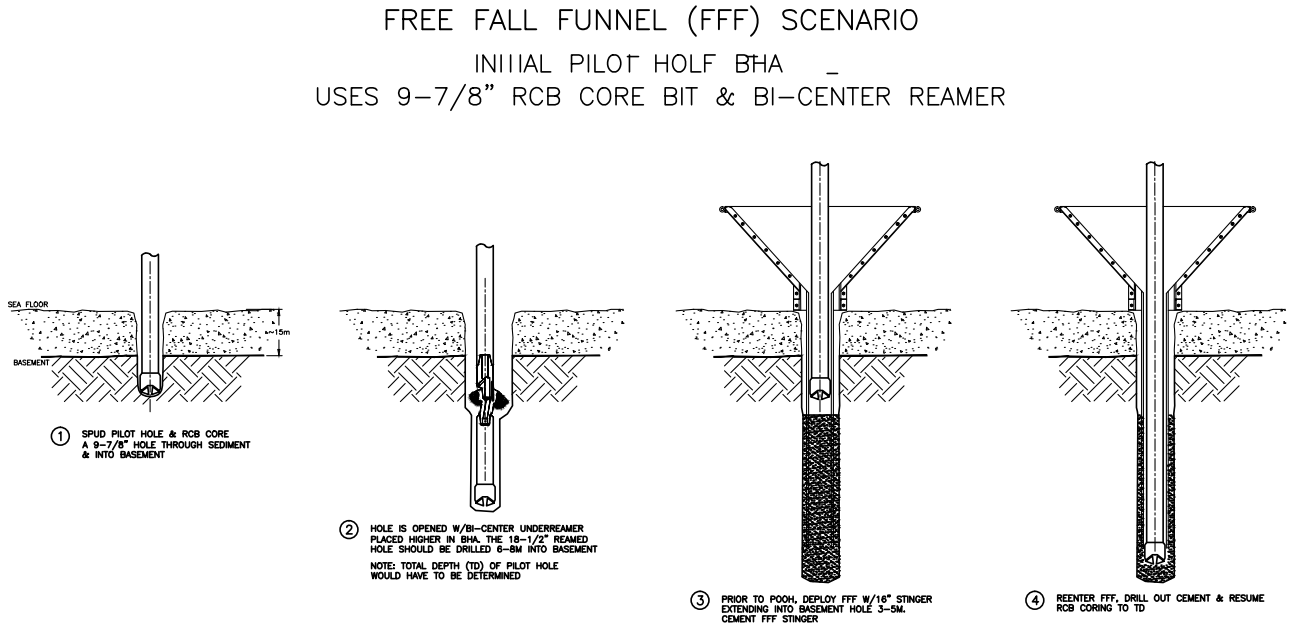

Figure F11. Schematic cartoon of a hole opener (underreamer or bi-center reamer) used for initiating a borehole that creates a larger hole near the seafloor. This might facilitate bare-rock re-entry and/or installation of a seafloor structure. See **"Drilling strategy and operations plan"** for explanation of operational approaches to be used to address expected drilling challenges.

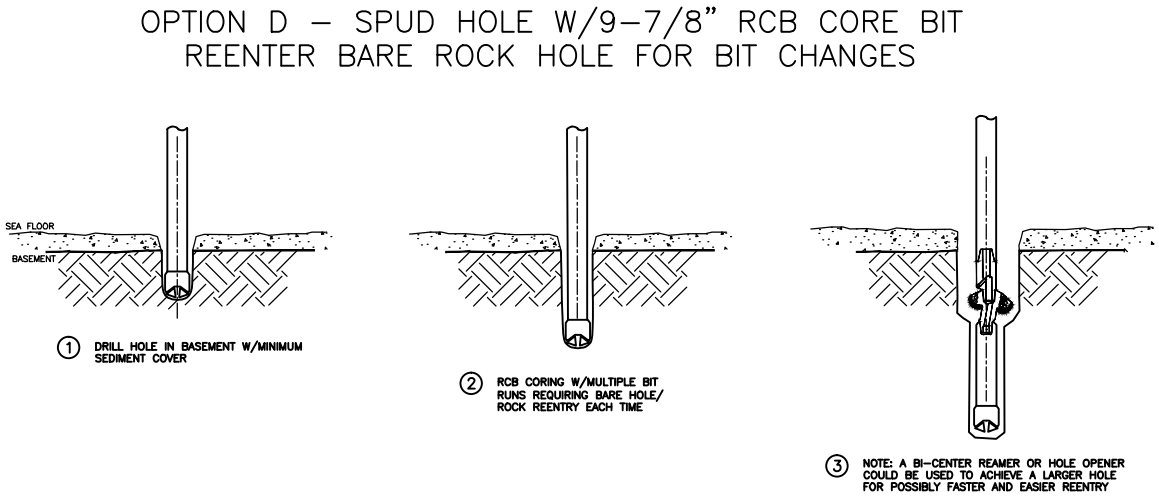

Site summaries

Site HB-01B

Priority:	Primary
Position:	2°15.175′N, 101°32.570′W
Water depth (m):	4855
Target drilling depth (mbsf):	≥265
Approved maximum penetration (mbsf):	Requesting no limit to penetration; pending IODP Environmental Protection and Safety Panel (EPSP) and Texas A&M Safety Panel (TAMU SP) approval
Survey coverage:	See Figure **AF1**
Objective(s):	Recover core and logs of lower crust
Drilling program:	RCB core and downhole logging as deep as possible; seafloor structure and casing as required to achieve this objective
Logging program:	• Triple combo • FMS-sonic
Nature of rock anticipated:	Gabbro

Site summaries (continued)

Site HB-02B

Priority:	Primary
Position:	2°15.138′N, 101°32.750′W
Water depth (m):	4860
Target drilling depth (mbsf):	≥265
Approved maximum penetration (mbsf):	Requesting no limit to penetration; pending IODP Environmental Protection and Safety Panel (EPSP) and Texas A&M Safety Panel (TAMU SP) approval
Survey coverage:	See Figure **AF1**
Objective(s):	Recover core and logs of lower crust
Drilling program:	RCB core and downhole logging as deep as possible; seafloor structure and casing as required to achieve this objective
Logging program:	• Triple combo • FMS-sonic
Nature of rock anticipated:	Gabbro

Site summaries (continued)

Site HB-03B

Priority:	Primary
Position:	22°15.138′N, 101°32.90′W
Water depth (m):	4855
Target drilling depth (mbsf):	≥265
Approved maximum penetration (mbsf):	Requesting no limit to penetration; pending IODP Environmental Protection and Safety Panel (EPSP) and Texas A&M Safety Panel (TAMU SP) approval
Survey coverage:	See Figure **AF1**
Objective(s):	Recover core and logs of lower crust
Drilling program:	RCB core and downhole logging as deep as possible; seafloor structure and casing as required to achieve this objective
Logging program:	• Triple combo • FMS-sonic
Nature of rock anticipated:	Gabbro

Site summaries (continued)

Site HB-04B

Priority:	Alternate
Position:	2°18.05′N, 101°31.55′W
Water depth (m):	3050
Target drilling depth (mbsf):	≥265
Approved maximum penetration (mbsf):	Requesting no limit to penetration; pending IODP Environmental Protection and Safety Panel (EPSP) and Texas A&M Safety Panel (TAMU SP) approval
Survey coverage:	See Figure **AF2**
Objective(s):	Recover core and logs of lower crust
Drilling program:	RCB core and downhole logging as deep as possible; seafloor structure and casing as required to achieve this objective
Logging program:	• Triple combo • FMS-sonic
Nature of rock anticipated:	Gabbro

Figure AF1. Summary of site survey data used to select primary proposed Sites HD-01B–HD-03B. **A.** Regional contoured bathymetric map of the Hess Deep Rift with locations of primary and alternate proposed sites and ODP Sites 894 and 895. Contour intervals = 100 m. Black box identifies the area enlarged in B; dashed north–south line indicates the location of the seismic reflection profile shown in C. **B.** Contoured microbathymetry map with locations of primary proposed drill sites and the distribution of rock types recovered by the ROV *Isis*. Contour interval = 20 m. **C.** North–south trending multichannel seismic reflection across the Hess Deep Rift. Line HD207 was collected during Cruise EW0305 on board the R/V *Ewing* in 2003 (G. Christensen, unpubl. data). The poor quality of the profile caused by the extreme topography at the Hess Deep Rift, therefore these data were not used to select the primary drill sites. **D.** Seafloor image of the sedimented bench on which proposed Sites HD-01B–HD-03B are located. **E.** Photo of a hand specimen of olivine gabbro collected from within 100 m of proposed Site HD-02B. **F.** Seafloor photo of an olivine gabbro outcrop located 100 m south of proposed Site HD-01B. Width of photo = ~1 m.

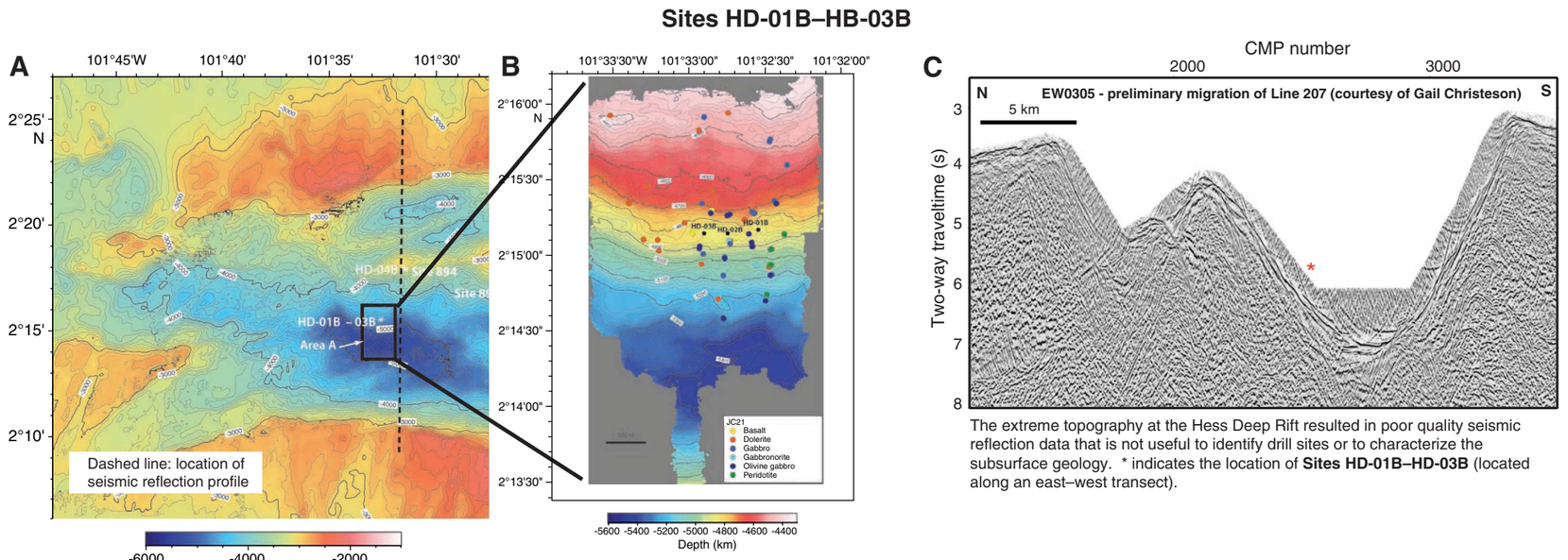

The extreme topography at the Hess Deep Rift resulted in poor quality seismic reflection data that is not useful to identify drill sites or to characterize the subsurface geology. * indicates the location of **Sites HD-01B–HD-03B** (located along an east–west transect).

ROV image of sedimented surface of bench surrounding proposed drill sites.

Olivine gabbro located within 100 m of **Site HB-02B.**

Photo taken from ROV *Isis* of olivine gabbro outcrop; outcrop is located 100 m south of **Site HD-01B**. Width of photo ~1 m.

Figure AF2. Summary of the site survey data used to select the alternate proposed Site HD-04B. **A.** Regional contoured bathymetric map of the Hess Deep Rift with locations of the primary and alternate proposed sites and ODP Sites 894 and 895. Contour intervals = 100 m. Black box identifies the area enlarged in B; dashed north–south line indicates the location of the seismic reflection profile shown in C. **B.** Contoured bathymetry map with location of alternate proposed site and the distribution of rock types recovered by the ROV *Isis*. Contour interval = 100 m. **C.** North–south trending multichannel seismic reflection across the Hess Deep Rift. Line HD207 was collected during Cruise EW0305 on board the R/V *Ewing* in 2003 (G. Christensen, unpubl. data). The poor quality of the profile is caused by the extreme topography at the Hess Deep Rift, therefore these data were not used to select the alternate drill sites.

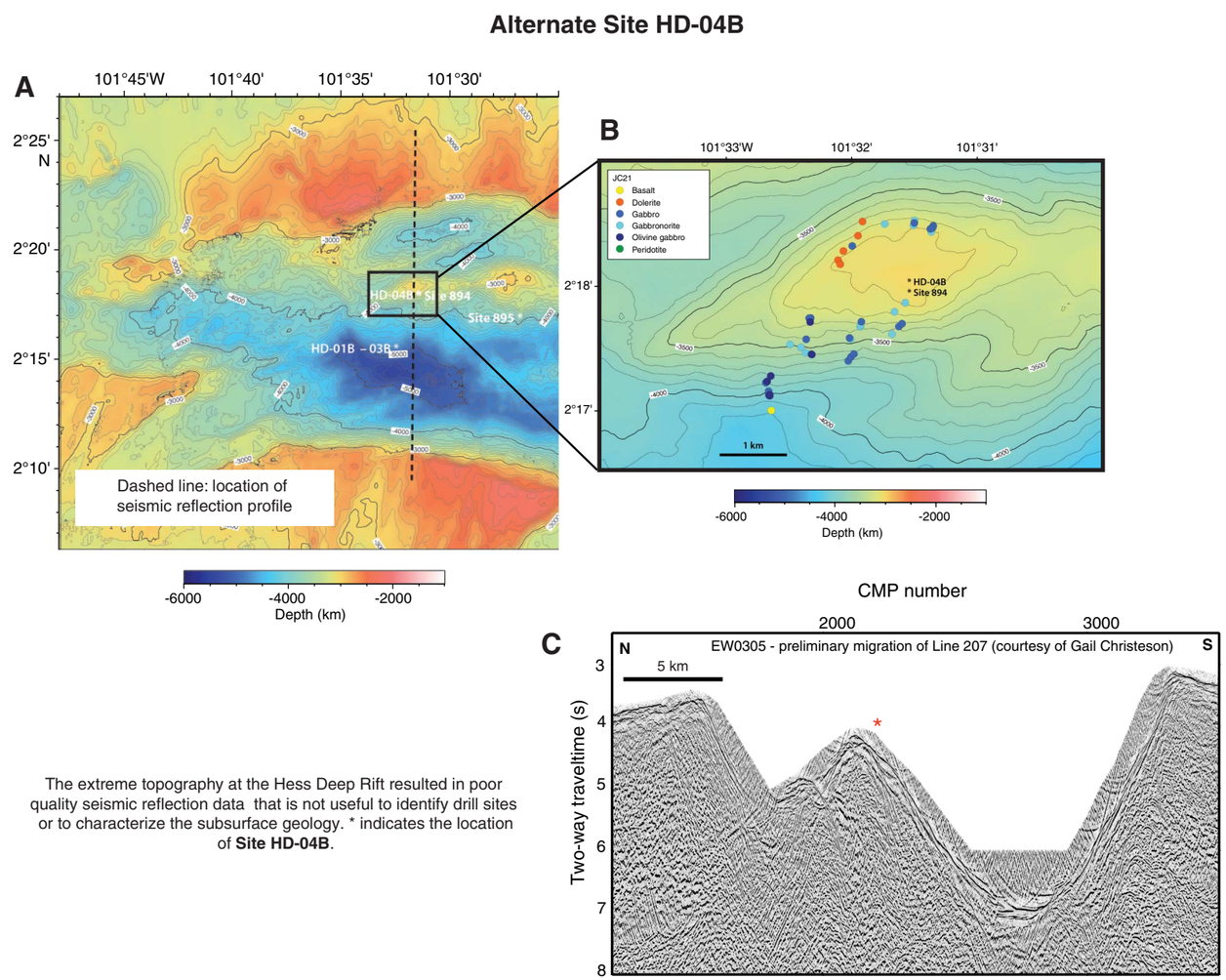

Expedition scientists and scientific participants

The current list of participants for Expedition 345 can be found at **iodp.tamu.edu/scienceops/expeditions/hess_deep.html**